Fünfter Interdisziplinärer Workshop Maritime Systeme

Aktuelle Ergebnisse aus laufenden Promotionsprojekten an der TUHH

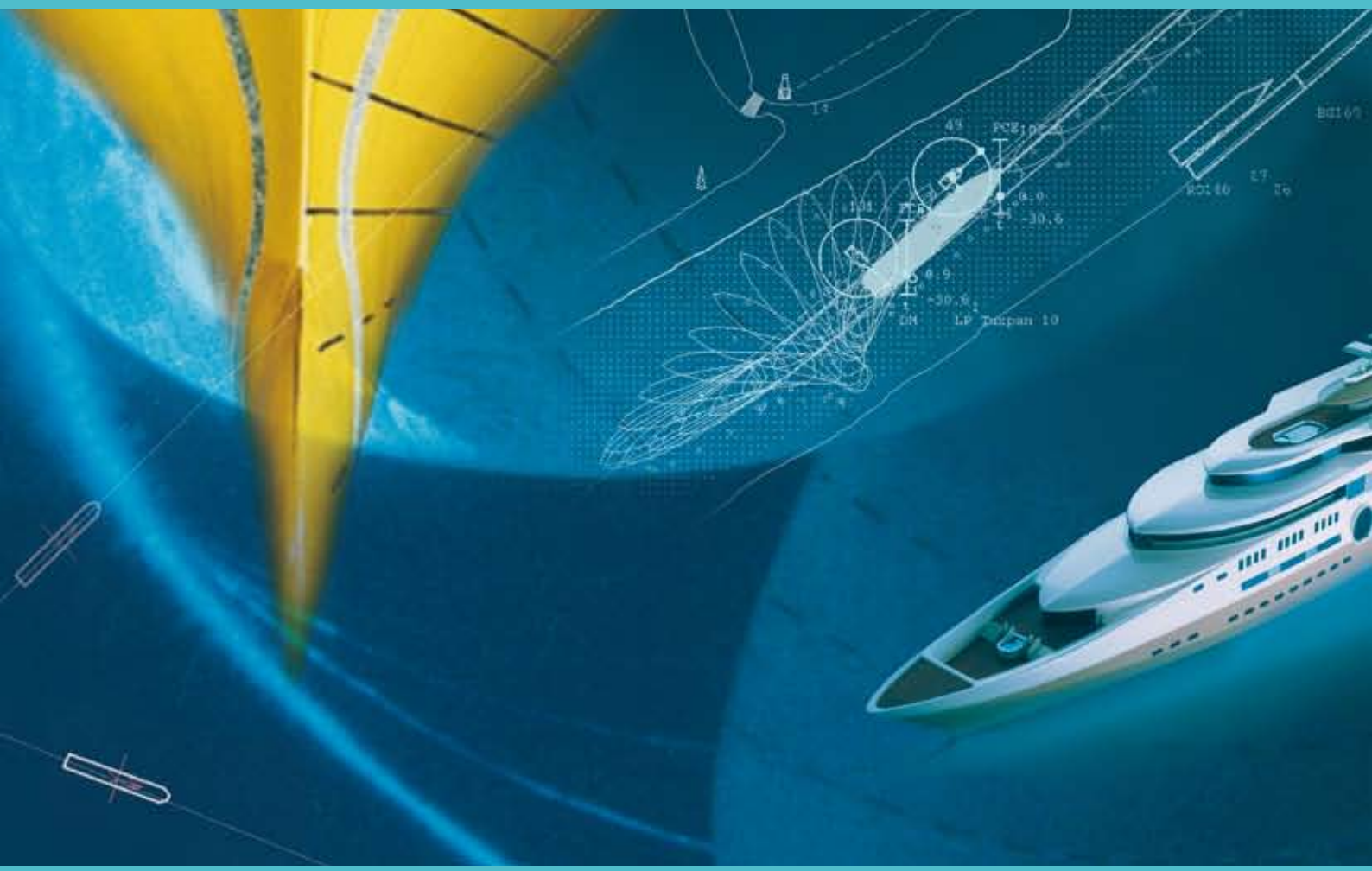

TUHH

Technische Universität Hamburg-Harburg

Fünfter Interdisziplinärer Workshop Maritime Systeme

Aktuelle Ergebnisse aus laufenden Promotionsprojekten an der TUHH

Hamburg, 02.Februar 2014

TUHH
Technische Universität Hamburg-Harburg

Impressum

Herausgeber
Forschungsschwerpunkt Maritime Systeme der TUHH

Redaktion
Sven-Brian Müller

Gestaltung
Formlabor, Hamburg

Inhalt

Produktivitätsanalyse in der Unikatfertigung mit mobilen Endgeräten

Florian Tietze, Hermann Lödding
Technische Universität Hamburg-Harburg, Institut für Produktionsmanagement und -technik, Denickestraße 17, 21073 Hamburg, florian.tietze@tuhh.de

In der personalintensiven Unikatfertigung ist eine hohe Arbeitsproduktivität besonders wichtig. Vielfach fehlt jedoch die Transparenz über die Einflussfaktoren, um eine geeignete Verbesserungsmaßnahme festzulegen. Zwar steht eine Vielzahl von Analysemethoden aus dem Produktivitätsmanagement und der schlanken Produktion zur Verfügung, um Transparenz zu schaffen. Die Besonderheiten der Unikatfertigung erschweren jedoch die Anwendung und führen häufig zu einem erheblichen Analyseaufwand. Mit Hilfe von mobilen Endgeräten ist es möglich, den Erhebungsaufwand zu reduzieren. Dazu müssen jedoch die Analysemethoden angepasst oder neu entwickelt werden.

1 Einleitung

Die Produktivität ist allgemein definiert als das Verhältnis von Output zu Input eines Produktionsprozesses [1]. Die Arbeitsproduktivität bezieht sich auf die Ressource Mensch als Inputfaktor und lässt sich beispielweise als Verhältnis der produzierten Vorgabestunden (Output) zu den bezahlten Arbeitsstunden (Input) definieren.

2 Handlungsorientierte Produktivitätsanalyse in der Unikatfertigung

Die Arbeitsproduktivität in der Unikatfertigung zu analysieren ist oftmals schwieriger als in der Serienfertigung: Zum einen haben die Mitarbeiter eine größere Aufgabenvielfalt und sind dadurch häufiger mit Nebentätigkeiten beschäftigt [2]. Zum anderen wiederholen sich die Prozesse in der Unikatfertigung kaum, wodurch die Anwendung von in der Serienfertigung üblichen Methoden wie z.B. Methods-Time Measurement und Zeitaufnahmen wenig sinnvoll erscheint [3]. Zusätzlich haben indirekte Bereiche wie z.B. Konstruktion und Arbeitsvorbereitung einen entscheidenden Einfluss auf die Produktivität und müssen mitberücksichtigt werden [4].

2.1 Definition von Mitarbeiterzuständen

Grundlage für die Analyse der Arbeitsproduktivität ist die Modellierung der Mitarbeiterzeit [5]. Dabei können die vielfältigen Aufgaben der Mitarbeiter in der Unikatfertigung mit Hilfe von Tätigkeiten und Objekten beschrieben werden [6]. Sowohl die Tätigkeiten als auch die Objekte sind übergeordneten Kategorien zugeordnet. Dabei orientieren sich die Tätigkeitskategorien an einem generischen Arbeitszyklus mit fünf Phasen: Informationsbeschaffung und -verarbeitung, Material- und Hilfsmittelbeschaffung, Bauteil- und Bauplatzvorbereitung, Durchführung, Nachbereitung. Die Objekte werden sechs Kategorien zugeordnet: Personen; Auftragsunterlagen, Transportmittel, Betriebsmittel, Hilfsmittel, Material/Werkstück. Aus der Kombination der Tätigkeits- und Objektliste ergibt sich eine Tätigkeits-Objekt-Matrix, die auszugsweise in Abbildung 1 dargestellt ist.

				1				2				3				...
				Informations-beschaffung und verarbeitung				Material- und Hilfsmittel-beschaffung				Bauteil- und Bauplatz-vorbereitung				...
				1	2	3	4	1	2	3	4	1	2	3	4	...
				lesen	betrachten	sprechen mit	...	transportieren	beladen	entladen	...	rüsten	auspacken	handhaben	...	...
1	Personal	1	Konstrukteur			x										
		2	Fertigungsing.			x										
		3	Meister			x										
		4	...			x										
2	Arbeits-unterlagen	1	3D-Viewer	x								x				
		2	Stückliste	x								x				
		3	Zeichnung	x								x				
		4	...	x								x				
...	⋮	...	...													

12512

Abb.1: Auszug aus einer Tätigkeits-Objekt-Matrix

Zur Vereinfachung sind die Objekte und Tätigkeiten mit Nummern codiert. Zusammen definieren ein Objektschlüssel und ein Tätigkeitsschlüssel einen Mitarbeiterzustand. Die möglichen Kombinationen von Tätigkeiten und Objekten sind mit einem Kreuz markiert.

2.2 Aufnahmemethoden

Als Aufnahmemethode in der Unikatfertigung eignen sich vor allem die Multimomentaufnahme und Prozessaufnahmen. Bei Multimomentaufnahmen notiert der Anwender zu definierten Zeitpunkten auf Rundgängen durch den Untersuchungsbereich die Mitarbeiterzustände. Eine Vielzahl von Stichproben muss erhoben werden, um mit ausreichender statistischer Sicherheit die mittels Stichproben erhobenen Mittelwerte auf die Grundgesamtheit übertragen zu können [7]. Ergebnis sind Mitarbeiterzustandsanteile bezogen auf den Aufnahmezeitraum. Es ist möglich, größere Produktionsbereiche mit relativ geringem Aufwand zu analysieren und dabei die Mitarbeiter nur geringfügig zu stören. Dazu ist es häufig notwendig, deutlich mehr als 1000 Stichproben aufzunehmen.

Bei Prozessablaufanalysen nimmt der Anwender den gesamten Prozessablauf standardisiert auf und notiert die Dauern und Reihenfolge der Mitarbeiterzustände. Dazu ist es notwendig, den gesamten Prozess zu begleiten, so dass der Aufwand relativ hoch sein kann.

Die Datenerfassung kann entweder durch Fremd- oder Selbstaufschreibung erfolgen. Um einen Mitarbeiterzustand aufzunehmen, trägt man den entsprechenden Tätigkeits- und Objektcode in den Aufnahmebogen ein, wie er in Abbildung 2 dargestellt ist.

Uhr-zeit	Objektelement			Tätigkeitselement			Bemerkung
	Kat.	Obj.	Bezeichnung	Kat.	Tät..	Bezeichnung	
8:47	2	3	Zeichnung	1	1	lesen	
9:12	1	1	Konstrukteur	1	3	sprechen	Rückfragen bzgl. Zeichnung
...	...	...	...	...	...	...	...

12413

Abb.2: Beispiel eines Datenaufnahmebogens

In der Praxis hat sich gezeigt, dass sich Multimomentaufnahmen mit Beobachtern für übersichtliche Produktionsbereiche sehr gut eignen. In indirekten Bereichen können Beobachter aufgrund der Aufgabenvielfalt und der immateriellen Leistungserstellung kaum Tätigkeiten und Objekte der Mitarbeiter identifizieren. Daher ist es sinnvoll, dass die Mitarbeiter die Daten selbst aufnehmen. Unternehmen sollten standardisierte Aufnahmebögen oder Software benutzen, um den Erhebungsaufwand und mögliche Fehler zu reduzieren.

3 Mobile Endgeräte bei der Datenaufnahme

In der Serienfertigung ist der Einsatz von mobilen Endgeräten und Software zur Analyse der Arbeitsproduktivität üblich. Sowohl speziell entwickelte mobile Endgeräte [8] als auch Applikationen für handelsübliche Tablet-Computer [9, 10] stehen zur Verfügung. Da die Produktivitätsanalysen in der Unikatfertigung häufig nicht anwendbar sind, ist der Einsatz von mobilen Endgeräten und Software kaum möglich. Am IPMT wurde eine Software für die Durchführung von Produktivitätsanalysen in der Unikatfertigung entwickelt.

3.1 Integration mobiler Endgeräte in die handlungsorientierten Produktivitätsanalyse

Die Software unterstützt die Datenaufnahme und ermöglicht es, die Tätigkeiten und Objekte zur Beschreibung der Mitarbeiterzustände mit einem Tablet-Computer aufzunehmen und in Excel automatisiert auszuwerten. Sowohl Multimomentaufnahmen als auch Prozessablaufanalysen werden unterstützt. In einem ersten Schritt ist es notwendig, die Tätigkeits-Objekt-Matrix anzupassen. Dazu kann der Anwender in einer Excel-Datei Tätig-keiten und Objekte umbenennen oder hinzufügen. Ein Visual-Basic-Makro erzeugt aus der Tätigkeits-Objekt-Matrix eine xml-Datei, die der Anwender auf einen Tablet-Computer mit dem Betriebssystem Android übertragen muss. In der xml-Datei sind alle Tätigkeiten und Objekte, die übergeordneten Kategorienamen sowie die gültigen Kombinationen beschrieben. In der Applikation auf dem Tablet-Computer kann der Anwender auf verschiedene Tätigkeits-Objekt-Matrizen zugreifen, um verschiedene Bereiche zu untersuchen. Notwendige Daten für die Multimomentaufnahme oder die Prozessaufnahme, wie die Anzahl der Rundgänge und die Beobachtungspunkte oder zusätzliche Kommentare für die Aufnahme, trägt der Anwender direkt bei der Aufnahme am Tablet-Computer ein. Die eigentliche Datenaufnahme erfolgt durch wenige Klicks auf die angezeigten Tätigkeiten und Objekte. Dabei erfolgt sowohl eine Gültigkeitskontrolle, so dass keine ungültigen Kombinationen ausgewählt werden können, als auch eine automatische Zuordnung der Daten zu Zeitpunkten oder Aufnahmeorten. Die Da-

ten werden in csv-Dateien gespeichert. Die Auswertung der Aufnahmen erfolgt mit Excel. Dazu können die Daten über ein Visual-Basic-Makro eingelesen und in Pivot-Tabellen automatisiert ausgewertet werden.

3.2 Fallstudie

Ein Beispiel aus der Industrie zeigt die Anwendung der Methode auf eine Fertigung in der schiffbaulichen Unikatfertigung. Die Fertigung ist übersichtlich organisiert, so dass als Aufnahmemethode die Multimomentaufnahme möglich war. Gespräche mit einem Meister und einem Vorarbeiter sowie eine Begehung des Untersuchungsbereichs waren notwendig, um die Tätigkeits-Objekt-Matrix anzupassen. Insgesamt betrug der Anpassungsaufwand weniger als zwei Stunden. Zwei Beobachter nahmen mit Tablet-Computer und der IPMT-Software insgesamt 1530 Mitarbeiterzustände auf. Der Zeitaufwand für die Aufnahmen betrug insgesamt 16 Stunden und konnte gegenüber einer schriftlichen Aufnahme wesentlich reduziert werden. Die häufigsten Tätigkeiten und Objekte sowie die Mitarbeiterzustände mit dem größten Anteil an der Anwesenheitszeit sind in Tabelle 1 dargestellt.

Tab. 1: Auswertung der häufigsten Tätigkeiten, Objekte und Mitarbeiterzustände

Schiffbauliche Unikatfertigung						
Rang	Objekt	Anteil	Tätigkeit	Anteil	Mitarbeiterzustand	Anteil
1	Werkstück	37%	schweißen	13%	schweißen Werkstück	13%
2	Mitarbeiter	14%	betrachten	12%	sprechen mit Mitarbeiter	9%
3	Sektion	12%	sprechen mit	11%	ausrichten Werkstück	7%
4	Zeichnung	11%	transportieren	11%	montieren Werkstück	6%
5	Schweißgerät	6%	gehen zu	10%	betrachten Zeichnung	5%
Σ		80%		57%		34%

12511

3 Zusammenfassung

Der Einsatz von mobilen Endgeräten zur Analyse der Produktivität in der Unikatfertigung ist sinnvoll. Es ist möglich, den Datenerhebungsaufwand sowie die den Auswertungsaufwand erheblich zu senken.

Danksagung

Das Forschungsprojekt PROSPER wurde gefördert vom Bundesministerium für Forschung und Technologie (BMWi) aufgrund eines Beschlusses des Deutschen Bundestages.

Literaturverzeichnis

[1] Bokranz, R.; Landau, K.: Produktivitätsmanagement von Arbeitssystemen. Stuttgart: Schäffer-Poeschel, 2006.
[2] Gruß, R.: Schlanke Unikatfertigung – Zweistufiges Taktphasenmodell zur Steigerung der Prozesseffizienz in der Unikatfertigung auf Basis der Lean Production. Wiesbaden, 2010.
[3] Hirsch, B.E.: CIM in der Unikatfertigung und -montage. Berlin, Köln, 1992.
[4] Kuhlmann, T.: Konzeption und Entwicklung eines Systems zur Koordinierung der Produktion komplexer Unikate. Dissertation, Bremen, 1994.
[5] Czumanski, T.; Lödding, H.: Analyse von Einflussfaktoren auf die Arbeitsproduktivität in der Serienproduktion. In: Müller, E. (Hrsg.): Demografischer Wandel - Herausforderung für die Arbeits- und Betriebsorganisation der Zukunft. HAB-Forschungsbericht 2013, S. 237-261.
[6] Frühwald, C.: Analyse und Planung produktionstechnischer Rüstabläufe. Düsseldorf, 1990.
[7] Simons, B.: Das Multimoment-Zeitmeßverfahren – Grundlagen und Anwendung. Köln, 1987.
[8] Refa Chronos (n.d.) [Online]. Verfügbar unter: http://www.refa.de/timetools/refa-chronos [27.01.2014].
[9] MTMmobile (n.d.) [Online]. Verfügbar unter: https://www.dmtm.com/software/produkte/mtmmobile/ [27.01.2014].
[10] Ortim c6 (n.d.) [Online]. Verfügbar unter: http://www.dmc-ortim.de/de/produkte/geraete-c-serie/ortim-c6.html [27.01.2014].

Investigation on the load carrying behaviour of windows subjected to dynamic loads

Wolfgang Fricke, Bjarne Gerlach, Matthias Guiard
Hamburg University of Technology, Institute for Ship Structural Design and Analysis, Schwarzenbergstraße 95 c, 21073 Hamburg, matthias.guiard@tuhh.de

Ship windows are often exposed to dynamic loads, e.g. impact loads. Therefore a research project was initiated in order to analyze the load carrying behaviour of windows subjected to dynamic loads. In the research project experimental drop tests were performed and compared to finite element calculations using smoothed particle hydrodynamics for fluid simulation. Even though results are conservative, the approach turned out to be suitable to calculate stresses in the window.

1 Introduction

Large windows are often arranged in modern ship hulls and superstructures. During the recent years, several accidents with catastrophic consequences due to failure of windows have been reported. Well-known examples of ships being struck by window failure are the cruise liners Louis Majesty and Bremen or the Offshore Supply Vessel VOS Sailor. These accidents have in common that windows did not resist the impact of large waves.

Loads on ship windows due to wave impact as well as the influence of the surrounding structure on the ultimate strength of the window are widely unknown. In conclusion, a research project focusing on the ultimate strength of ship windows under lateral load was started.

In order to gain more knowledge, four drop tests with water filled rubber bags on ship structures consisting of a laminated safety glass window bonded to a stiffened steel plate were carried out. The experimental results were compared with calculations in the time domain where the ship structure including the window is modelled with finite elements and the water is simulated with smoothed particles in LS-DYNA.

2 Experimental drop tests

Four drop tests were carried out with one test model. The test model is designed like a typical front bulkhead which might be subjected to impact loads by green water in heavy sea condition. The model includes a bonded 900 mm x 900 mm laminated safety glass window consisting of two panes, each 15 mm thick, laminated with PVB. The design pressure of the window is 80 kPa according to design rules [1].

The drop tests were carried out by dropping water-filled rubber bags from a crane on the test model. The drop height started with 8 m and was then raised up to 20 m. The mass of water was increased from 600 kg to 1000 kg. The experiments were intended to measure the response of the structure when the glass stays intact as well as in the event of failure. The load in the experiment is meant to be a defined load for simulation purpose and not to be correlated with a specific wave.

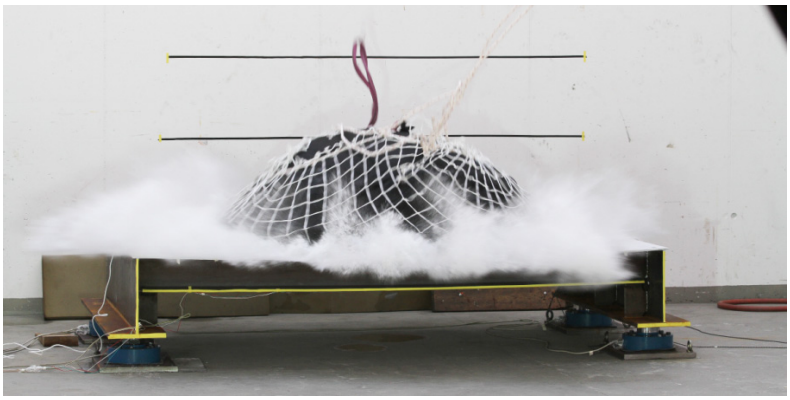

Fig. 1: Rubber bag at the moment of impact

The reaction force was measured with four load cells, strains in the middle of the lower side of the glass pane were measured with a strain gauge rosette in order to analyze the biaxial stress state. Another strain gauge was placed on top of a stiffener. All measurements were carried out with a sample rate of 100 kHz. The experiment

was recorded with two high-speed cameras. Tab. 1 gives an overview on the test parameters and the window state – intact or broken – after the test.

Tab. 1: Test parameter

test	height (m)	mass (kg)	speed (m/s)	glass intact/broken
1	8	600	12.5	intact
2	8	1000	12.5	intact
3	8	1000	12.5	intact
4	20	1000	19.5	broken

3 Numerical calculations

The drop tests were accompanied by numerical calculations with the explicit finite element software LS-Dyna. The steel structure as well as the glass was modelled with shell elements. Smoothed particle hydrodynamics (SPH) were used to model the water while the rubber bag was neglected. The bonding was replaced by shell elements with equivalent stiffness exhibiting linear-elastic material behaviour. The water was defined with an equation of state according to Grüneisen [2]. The surrounding steel structure was modelled with linear-elastic-plastic material behaviour. Fig. 2 shows the finite element model with SPH elements at the moment of impact.

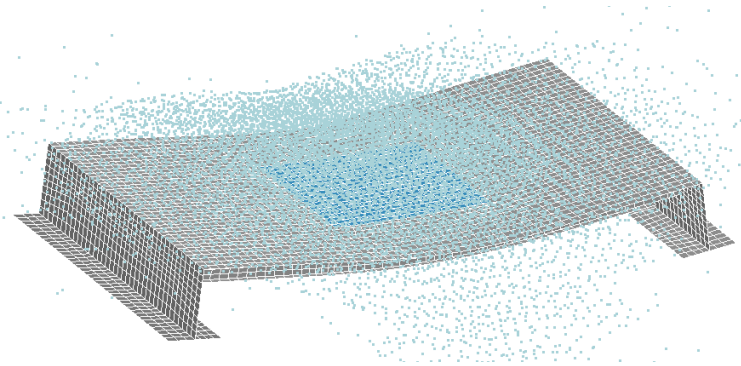

Fig. 2: FE Model in LS-DYNA with Smoothed Particles (SPH) to simulate the water

4 Comparison of experimental and numerical results

The comparison of experimental and calculation results showed that the influence of the specific boundary and initial conditions on the maximum values as well as on the distribution over time is significant. At first, the shape of the water volume was idealized as a box (which was the intended shape during manufacture of the rubber bag). For test 2, Fig. 3 shows that in this case calculated reaction forces are almost twice as high as measured.

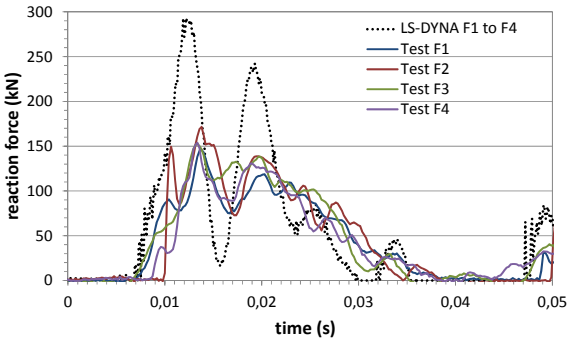

Fig. 3: Measured and calculated reaction forces F1 to F4 for test 2 with box shaped water

To consider the experimental conditions more accurately, water shape and position relative to the test model were adjusted with the help of videos and photos. Fig. 4 shows reasonable but not perfectly coinciding results for the reaction force after adjusting the initial conditions of the water. Obvious is that calculated peak values still

exceed the measured ones. Calculated values also show a higher rate of oscillation. The reason for that is not clear yet.

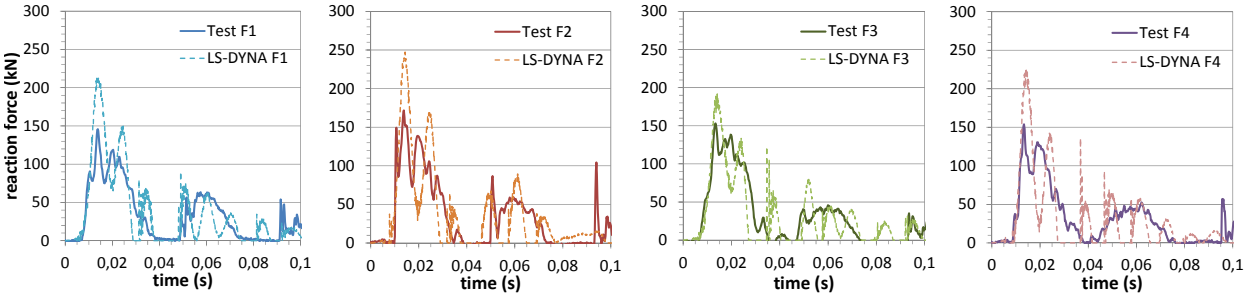

Fig. 4: Measured and calculated reaction forces F1 to F4 for test 2 with adjusted water shape

A better correlation between test data and calculation results can be found for the stresses in the glass pane at the lower side of the window (Fig. 5), however calculated maximum stresses are still higher than measured ones. Stresses in the glass reached the lower bound of the breaking strength range of safety glass which extends from about 150 MPa to 250 Mpa [3] [4]. Thus the glass could have been broken, but it did not. Strain rate effects may have led to a higher breaking strength.

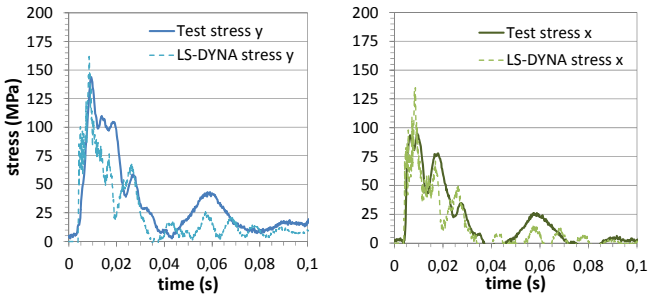

Fig. 5: Measured and calculated stresses in the glass pane on the bottom side for test 2 with adjusted water shape

5 Conclusion

In the outlined research projects the load-carrying behaviour of window structures was investigated experimentally and numerically. Experiments were carried out with impact loads realized by dropping water-filled rubber bags on a test model. The presented results point out that the structural reactions are sensitive to initial conditions like shape and relative angle of the approaching water mass. Comparison of reaction forces turned out that calculated peak values are higher than measured ones. The reason for that is not clear yet and subject of further investigations. Results are rather conservative, however, comparison of measured and calculated data for stresses show better correlation in respect of time and magnitude than for reaction forces. Thus the method turned out to be suitable for calculation of stresses in windows subjected to dynamic load for purpose of investigation on window failure and design optimization.

Acknowledgment

We gratefully acknowledge the support provided by the Free and Hanseatic City of Hamburg.

References

[1] GL: Rules for Classification and Construction, I Ship Technology, 1 Seagoing Ships 1 Hull Structures. Germanischer Lloyd, Hamburg, 2013.

[2] Fricke, W; Bronsart, R. (Eds.): Proceedings of the 18th International Ship and Offshore Structures Congress Volume 2, p. 48., Schiffahrts-Verlag “Hansa” GmbH & Co. KG, Hamburg, 2012.

[3] Haldimann, M.; Luible, A.; Overend, M.: Structural Use of Glass. IASBE-AIPC-IVBH, Zürich, 2008.

[4] Fricke, W.; Gerlach, B.; Guiard, M.: Structural behavior of large windows aboard ships (in German). Report 22/2013, Center of Maritime Technologies, Hamburg, 2013.

Viscous Multi-Body Hydrodynamics for Offshore Applications

Xiaojing Luo, Thomas Rung
Hamburg University of Technology, Institute of Fluid Dynamics and Ship Theory, Schwarzenbergstraße 95c, 21073 Hamburg, Germany, xiaojing.luo@tuhh.de

The report shows the applicability of advanced viscous flow simulation strategies to complex, full-scale marine-engineering problems. Results are shown for overset grid techniques supplemented by a quaternion-based motion modeller for (un)coupled floating bodies. Examples included refer to floating body and multi-body systems exposed to seaways as well as towing operations.

1 Introduction

For the assessment of the offshore capability of ships, it is important to consider their behaviour and characteristics when operating in seaway while taking the interaction with other floating or founded bodies into account. With regards to viscous flow-simulation approaches, the associated challenge beyond the state-of-the-art refers to (1) sea keeping and manoeuvring in seaways with transient heading, (2) the ability to mimic the hydrodynamic interaction of multiple floating bodies with large relative motions and (3) appropriate models for possible mechanical interactions of floating bodies - e.g. due to towing, launching or dynamic positioning.

2 Computational Models

The computational models described herein are implemented in the in-house finite volume solver FreSCo+, which solves the Navier-Stokes equations for an incompressible fluid composed of two (or more) immiscible phases. Various turbulence-closures are available with respect to statistical (RANS) or scale-resolving (LES, DES) approaches. Two-phase flows are addressed by interface-capturing methods based upon the Volume-of-Fluid (VoF) technique. More details are given by Rung et al. [5].

2.1 Overset Grid Method

When attention is directed to the second and third challenge, the geometric flexibility requirements on the simulation approach are substantial. Overlapping grid method, also referred to as overset/chimera grid methods, are a versatile method regarding complex moving geometries. The algorithm uses a background mesh defining the extents of the computational domain and a moving rigid foreground mesh associated with each moving body to model relative motion. In the grid transition region, at least two grids overlap. With this method very close arrangements of moving parts can be modelled. The present overset-grids technique refers to a mass-conservative, strongly coupled, fully parallelised approach as described by Brunswig et al. [1].

2.2 Seaway Model

When attention is drawn to manoeuvring and seakeeping simulations in waves, one challenge refers to the behaviour of the wave field downstream of the floating body, in particular the management of wave reflections induced at the outlet of the domain. Due to the inherent directionality, grid-based damping is not applicable if the wave direction changes in time, e.g. during offshore operations of vessels. Coupled viscous/inviscid methods are an attractive way to address these challenges. The technique employed here assumes that viscous and diffraction effects are negligible in the vicinity of the far-field boundaries. The coupling of both methods is achieved by an implicit forcing of the viscous solution using a manipulation of the coefficient matrix.

2.3 Motion Model

Floating-body motions follow from a motion modeller which converts the external and hydrodynamic forces exerted on the body into its motion. Quaternions - also known as Euler parameters - are employed for the motion modeller, in order to avoid singularities (i.e. effects of a *gimbal lock*) and ensure that each motion is uniquely defined.

In a multi-body arrangement, the motion model might have to consider additional constraints due to mechanical joints. The method aims to simulate constrained mechanical systems in which the components in the system are connected by non-redundant holonomic constraints. Common mechanical connection like spring-damper system, fender and rope, as well as translational joint and fixed distance between two points serve as baseline examples of coupled bodies. The motion modeller can be coupled to the momentum solver in an explicit, semi-implicit or implicit manner.

3 Examples and Applications

The resulting computational procedure has been applied to the numerical simulation of multibody systems in seaway. Examples included in this section refer to a collection of 3D floating bodies investigated by the overset-grid method. Emphasis is given to seaway aspects and mechanical coupling issues. For efficiency reasons all investigations were performed with fairly compact physical domains/background grids. Three examples are given in the following.

The first case refers to the simulation of a free-floating single rectangular box in complex seaway. The Jonswap seaway in Fig. 1 is composed of 200 components from different approach angles. The obstacle is pushed forward with a slight yawing motion by the dominating wave components and performs substantial heave and pitch oscillations. A particularly interesting point refers to the roll motion. As the density of the obstacle is assigned to half of water, the initial horizontal bottom floating position is not stable. A stable position is found at 45° rotation from the initial position, in line with theoretical results.

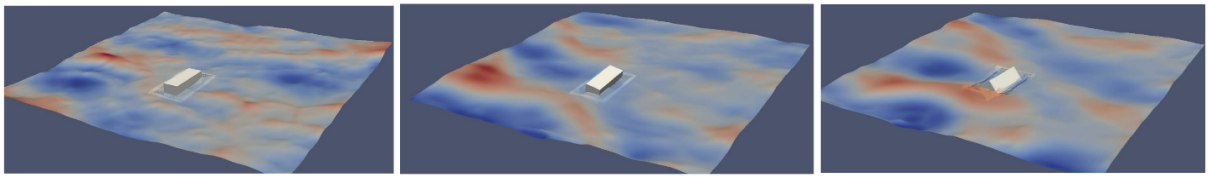

Fig. 1: Snapshots of overset-grid simulation for a semi-submerged box exposed to seaway

The second case is concerned with the sinking process of two coupled cylinders in harmonic seaways. As indicated by Fig. 2, the left cylinder, which is modelled from a very dense material, immediately sinks and pulls the right cylinder down. The overall motion is rather complex and again simulated in a fairly small domain.

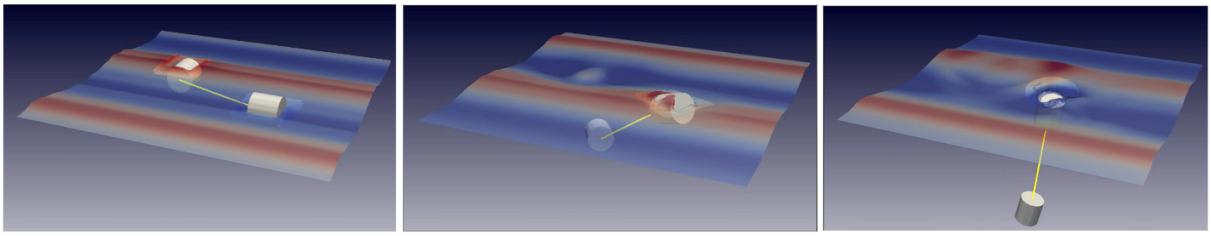

Fig. 2: Snapshots of overset-grid simulation for two sinking cylinders connected by a rigid link in waves

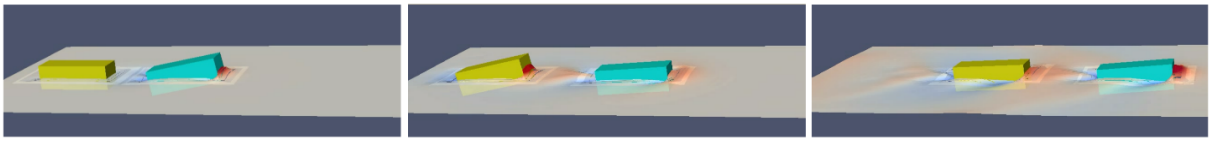

Fig. 3: Snapshots of overset-grid simulation for a generic towing operation

The last case shows the simulation of a generic towing scenario composed from two boxes in calm water. Again a similar computation setup was used. In Fig. 3 the right box is supplemented by an additional propulsion force and tows the left box from left to right. Mind that the use of the seaway model also supports the calm-water situation and the simulation runs stable even when the bow section of the towing box passes the external boundary to the background mesh.

Acknowledgment

We gratefully acknowledge the support provided by the Free and Hanseatic City of Hamburg.

References

[1] Brunswig, J.; Manzke, M.; Rung T.: Explicit and Implicit Coupling Strategies for Overset Grids. 10th Symp. on Overset Composite Grids and Solution Strategies, NASA AMES Res. Center, Moffett Field. September 2010.

[2] Luo, X.; Brunswig, J.; Manzke, M.; Koliha, N.; Matin, F.; Janßen, C.F.; Rung, T: Analyses of Coupled Floating Bodies in Seaway. 2nd International Conference on Violent Flows. Nantes, France. September 2012.
[3] Rung, T.; Luo, X.; Matin, F.: Multi-Body Hydrodynamics using Parallel Overset-Grid Technique. EC-COMAS MARINE 2013, Hamburg. 2013.
[4] Rung, T.; Ulrich, C.; Luo, X.: Multi-Body Hydrodynamics for Offshore Applications using Advanced Viscous Flow Simulation Techniques. Conference on Maritime Energy (COME), Hamburg. 2013.
[5] Rung, T.; Wöckner, K.; Manzke, M.; Stück, A.; Brunswig, L.; Ulrich C.: Challenges and Perspectives for Maritime CFD Applications. Jahrbuch Schiffbautechnische Gesellschaft, 103.

Numerical Simulation of Ship Collision with Gravity Base Foundation of Offshore Wind Turbine

David Osthoff
Hamburg University of Technology, Institute of Geotechnical Engineering and Construction Management, Harburger Schloßstraße 2, 21079Hamburg, Germany, david.osthoff@tuhh.de

For the installation of offshore constructions in Germany the evidence to prevent interference to the safety of shipping and unjustifiable impact on the environment is required. Especially the case of ship collision for gravity base foundations is problematic due to larger stiffness and mass compared to current steel-based offshore foundations. Using the finite element method a ship collision of a fully loaded double hull tanker and a gravity base foundation is simulated. Different water levels and the influence of swell are investigated as well as the damages to the vessel shown.

1 Introduction

In relation to the increasing role of renewable energies, various offshore wind energy parks in the European North and Baltic Sea are planned, under construction or already set up. For the installation of offshore constructions some countries, like Germany for example, require the evidence to prevent interference to the safety of shipping and unjustifiable impact on the environment (§ 3 SeeAnlV). For offshore wind parks the case of ship collision in particular has to be investigated as a loss of cargo or even the loss of the vessel affects both terms.

2 Approaches for the load case of ship collision

Ship and structure interactions are throughout interest of public as a failure may result in devastating consequences. Most studies focus on ship-to-ship collision or grounding. The collision of ship and offshore wind foundation is relatively new.

Extensive studies on the collision behaviour of ships and offshore wind foundations were performed by [1] using the finite element method. Different ship and foundation types are varied, although just offshore structures out of steel are part of the study like monopoles, tripods and jackets. In these cases the most damage derives from a disabled vessel drifting sideways against an offshore wind foundation due to the lower stiffness of the ship side walls. It has been shown that foundation structures with lower stiffness cause less damage to colliding vessels.

In order to investigate the influence of massive gravity base foundations the collision of a gravity base foundation and a single hull tanker are analyzed numerically in [4]. The foundation has a diameter of 40m and 30m respectively. The single hull tanker drifts horizontally as performed in [1]. Water level and embedment depth of the foundation are varied and the failure of steel is calculated. In every scenario the single hull tanker shows a total failure area of the ship´s hull of around 5 m². A discharge of supplies cannot be ruled out, the evidence of collision-safety regarding the gravity base foundation design cannot be provided.

3 Investigated scenarios

Because from 2015 on single hull tanker are no longer permitted worldwide, in this paper the collision of a fully loaded double hull tanker with a 6 MW offshore wind turbine is investigated. Besides this load case is assumed as worst-case scenario, no additional external loads such as wind and waves are considered [4].

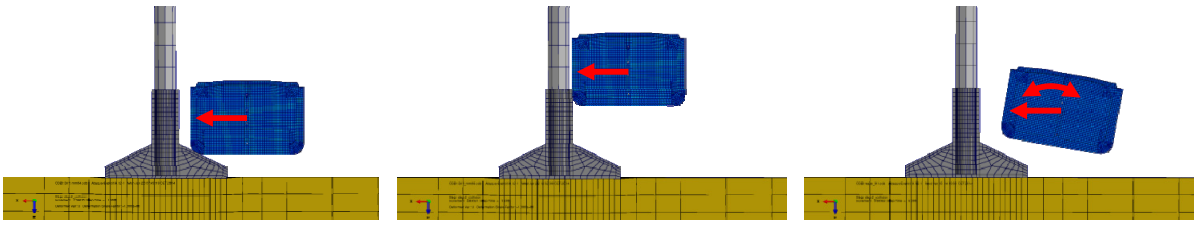

a) scenario 1
low water level

b) scenario 2
high water level

c) scenario 3
low water level and swell

Fig. 1: Investigated collision scenarios

The following three scenarios are simulated in order to evaluate the collision behaviour of the gravity base foundation, see Fig. 1. In all scenarios the vessel is drifting sideways in an angle of 90° against the foundation with a horizontal velocity of 2 m/s [1,2]. Further on in scenario 3 the influence of swell is simulated with a wave amplitude of 3 m at a time interval of 4 s. The heeling of the vessel due to rolling is assumed to ± 10°.

4 Numerical modelling

Three dimensional dynamic analyses are performed using the commercial finite element method (FEM) software Abaqus/Explicit 6.13. An explicit time integration algorithm is used. Due to further research just drained conditions can be applied on the sand.

4.1 Geometry and discretization

The finite element model is based on [1,4] and is shown in Figure 2. In order to reduce computational cost a plane of symmetry is applied on the model. The foundation has a diameter of 30 m and a height of 22 m. Sand works as ballast. Foundation and ballast are discretized with deformable 8-node continuum elements with reduced integration. For the tower on top of the foundation a diameter of 5 m and a height of 80 m are assumed [4]. The tower is discretized using 4-node shell elements with reduced integration and a thickness of 100 mm. The nacelle is modelled as a point mass possessing a mass moment of inertia. The assumed weight of the nacelle is 430 t. Nacelle and tower as well as tower and foundation are kinematically coupled in all degrees of freedom [4]. The region of the soil body depicts a diameter of 150 m and a height of 50 m and is modelled with continuum elements.

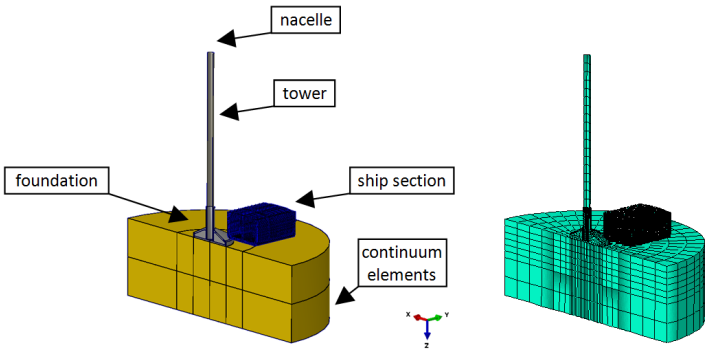

Fig. 2: Numerical model and discretization

The considered double hull tanker has a mass of 45,000 t, a length of 150 m, a width of 27.7 m and a height of 17.3 m. In a fully loaded state the average draft is approximately 10.5 m. In assumption the collision takes place in the exact middle of the vessel, the affected centre section is discretized using 4-node shell elements with reduced integration. The rest of the vessel is modelled as point mass including a mass moment of inertia. Besides the mass of the vessel is partly defined by the specific weight of steel, a further point mass considers facilities and cargo up to a fully loaded state. The vessel and all point masses are connected to a bearing point by all degrees of freedom, which is located in the centroid of the cross section. In order to consider buoyancy of the floating vessel, one linear spring in the vertical direction and one torsional spring about the vessel´s longitudinal axis are assembled in the bearing point.

The spring stiffness in vertical direction z and about the longitudinal axis of the vessel are calculated by:

$$k_z = \frac{m \cdot g}{h_0} \qquad (1) \qquad \text{and} \qquad k_\alpha = \frac{m \cdot g \cdot B^2}{12 \cdot h_0} \qquad (2)$$

where m is the mass of the modelled ship and h_0 the draft, see [5,6].

A motion of a vessel affects the surrounding water that is set in motion correspondingly. In case of an abrupt stop of a vessel by external forces, the surrounding water carries on in form of hydrodynamic mass. This additional mass is calculated according to [3] and is increasing proportionally with lower water depth.

In order to model swell two additional springs in linear and torsional direction are assembled in the bearing point. The swell is induced via stiffness and deflection. The springs simulating buoyancy are assembled in an additional reference point that is given the period defined in vertical and translational motion. In this way buoyancy acts when the motion of the vessel is not corresponding to the defined swell – here in case of collision.

4.2 Constitutive model and contact discretization

Constitutive models used in simulations as well as contact definitions are described in [4].

5 Deformation of the vessel

With first contact between vessel and foundation in scenario 1, a horizontal force is starting to act between both collision partners. If static friction in the contact surface of soil and foundation is exceeded, the foundation slides horizontally on the seabed. In consequence of frictional sliding and locally plastic deformation of the vessel´s hull and foundation surface, energy is dissipated as shown in Fig. 3. Due to the high stiffness of vessel and foundation the first contact causes an impact on the vessel, which is moving apart from contact surface. In this state buoyancy leads to a self aligning moment and vertical force and as result a second contact appears. The vessel then slips onto the cone of the foundation and is decelerating slowly up to stoppage. In the last phase of collision, the vessel drifts back from the foundation.

In scenario 2 at high water level the vessel drifts against the shaft of the foundation. The point of contact is higher above sea level and so the lever arm of contact force. Hence the foundation acts more rigid, its frictional sliding occurs less and the deceleration of the vessel is more rapid. Due to the smaller diameter of the shaft, the contact stresses are higher than in scenario 1.

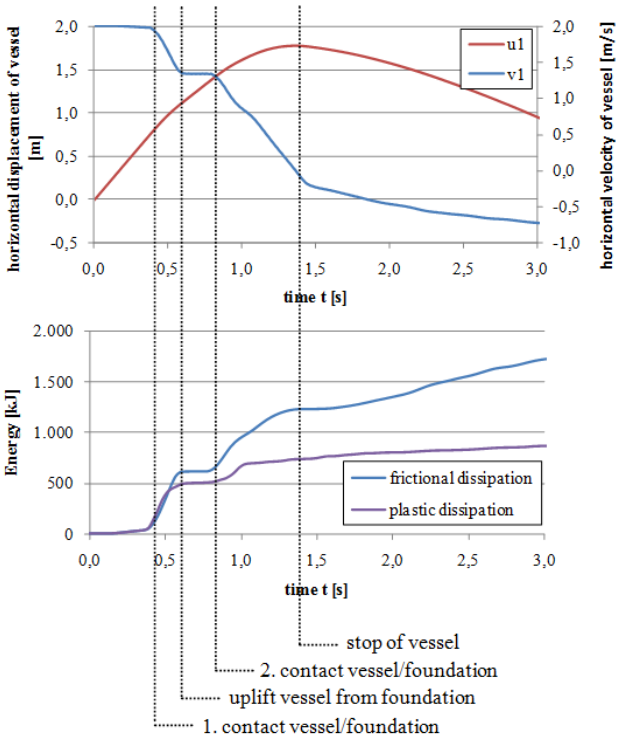

Fig. 3: Horizontal velocity and displacement of the vessel and dissipation of energy due to collision process; scenario 1

The influence of swell and therefore additional vertical plus rotational velocities are considered in scenario 3. The vessel impinged upon foundation at an angle of about 6°. The damage of the vessel resulting from collision is much higher than in scenarios 1 and 2. In Fig. 4 the remaining stress state according to van Mises is shown. Hence the damage due to swell is much higher, the damage to the vessel can be assumed as not critical for safety of vessel and supply.

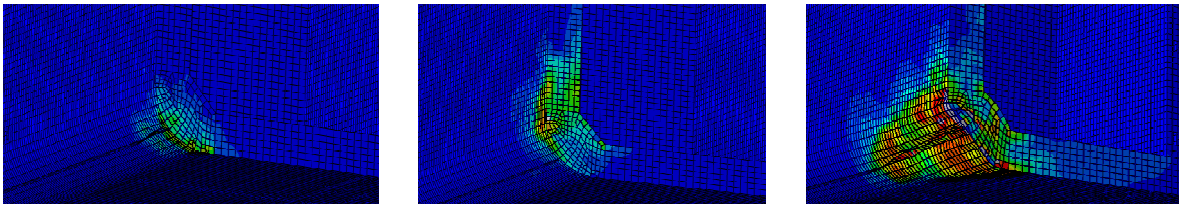

a) scenario 1 b) scenario 2 c) scenario 3

Fig. 4: Damages of the vessel´s hull after collision (Mises stress: 0 (blue) – 235 MPa (red))

For this type of foundation the influence of swell has to be varied further in order to detect boundaries of safety.

6 Conclusion

The collision of a double hull tanker with a gravity foundation is simulated numerically using the finite element method. The influence of water level and swell are investigated. With higher water level the foundation acts more rigid and the damage to the vessel increases. With consideration of swell further forces and moments are acting on the vessel. Therefore the impact calculated leads to a higher damage of the vessel. It can be shown that in these simulations the collision of the double hull tanker and the gravity base foundation leads to no critical damage to the vessel´s hull considering chosen design and boundary conditions.

Acknowledgment

We gratefully acknowledge the support provided by the Free and Hanseatic City of Hamburg.

References

[1] Biehl, F.: Kollisionssicherheit von Offshore-Windenergieanlagen. Dissertation, Institut für Konstruktion und Festigkeit von Schiffen, TU Hamburg-Harburg, Hamburg, 2009.

[2] Bundesamt für Seeschifffahrt und Hydrographie (BSH): Standard – Konstruktive Ausführung von Offshore-Windenergieanlagen, 2007.

[3] Grim, O.: Das Schiff und der Dalben. Schiff und Hafen, H.9, 1955.

[4] Hamann, T.; Pichler, T.: Numerical simulation of ship collision with gravity foundations of offshore wind turbines. In 32nd OMAE, 2013.

[5] Kauther, R.; Schuppener, B.: Physical modeling of ship collisions with waterway embankments. In 4th ICCGS, Hamburg, 2007.

[6] Qui, G.: Coupled Eulerian Lagrangian simulations of selected soil-structure interaction problems. Dissertation, Institut für Geotechnik und Baubetrieb, TU Hamburg-Harburg, Hamburg, 2012.

Leg-Seabed Interactions of Jack-Up Vessels

Edwin Kreuzer, Eugen Solowjow
Hamburg University of Technology, Institute of Mechanics and Ocean Engineering , Eißendorfer Straße 42, 21073 Hamburg, eugen.solowjow@tuhh.de

Gang Qiu, Thorben Hamann, Jürgen Grabe
Hamburg University of Technology, Institute of Geotechnical Engineering and Construction Management, Harburger Schloßstraße 20, 21079 Hamburg

This paper analyzes the leg-seabed interactions of a 3rd generation jack-up vessel in irregular waves due to vessel motions. The proposed model considers hydrodynamic forces on the hull as well as on the legs. The sea floor reaction forces are analyzed with a Coupled Eulerian-Lagrangian (CEL) method. The results are used to develop a mechanical rheological model for the sea floor. With computational efficiency in mind a state-space representation in time domain is derived. The excitation of the system is due to irregular waves, which are described by the JONSWAP spectrum. The proposed method allows the efficient computation of short term (2-15 min) scenarios and events through sampling of realizations. It is used to compute the impact forces on the legs from the seabed induced by irregular vessel motions. The presented framework is suitable for the planning of jack-up operations in the offshore wind industry. It can also be applied for the design of dynamic positioning and jacking systems.

1 Introduction

One of the key enablers for utilizing offshore wind farms as a primary source of renewable energy is the reduction of assembly and servicing times at sea. At depths of up to 50 meters jack-up vessels carry out many steps of the construction work. By providing operational limits for the grounding process of jack-up vessels, the construction of wind farms can become safer and more efficient. This paper analyzes the leg-seabed impacts of a jack-up vessel, due to the vessel's motion in irregular waves.

2 Jack-up Model

A generic 3rd generation jack-up vessel is used for the analysis. In the following, we consider zero forward speed and beam wave excitation. Beam waves will usually lead to the largest motion amplitudes. We restrict the degrees of freedom to sway, heave and roll, whereby heave and roll are coupled. Figure 1 shows the floating jack-up vessel.

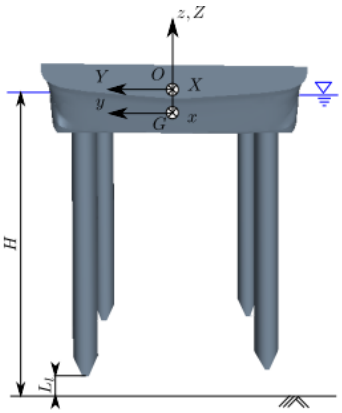

Fig. 1: Rear view of the analyzed jack-up vessel.

The linearized system of equations of motion in time domain can be formulated as:

$$\mathbf{M}\ddot{\boldsymbol{\xi}} = \mathbf{q}, \tag{1}$$

where $\mathbf{M}$ is the mass matrix of the rigid body and $\boldsymbol{\xi} = [\xi_2\ \xi_3\ \xi_4]^T$ the displacement vector (ξ_2-sway, ξ_3-heave, ξ_4-roll) with respect to an equilibrium frame. Assuming small vessel displacements and small wave amplitudes the force vector $\mathbf{q}$ can be decomposed in five components:

$$\mathbf{q} = \mathbf{q}_{\text{res}} + \mathbf{q}_{\text{rad}} + \mathbf{q}_{\text{exc}} + \mathbf{q}_{\text{legs}} + \mathbf{q}_{\text{seabed}}. \tag{2}$$

The first three components $\mathbf{q}_{\text{res}}$ $\mathbf{q}_{\text{rad}}$, $\mathbf{q}_{\text{exc}}$act on the hull and are the restoring, wave-radiation and wave-exciting forces, respectively. They correspond to the forces in Cummins' well-known equation [1]. The hydrodynamic

forces acting on the legs are described by $\mathbf{q}_{\text{legs}}$ and the forces resulting from leg-seabed interactions are given by $\mathbf{q}_{\text{seabed}}$.

2.1 Hydrodynamic Model

The hydrodynamic loads describe the fluid-structure interaction of the vessel. The required hydrodynamic coefficients depend on the vessel geometry and are computed with the strip theory.

For the radiation force we use a recently introduced method where the radiation force is approximated by a linear-time-invariant (LTI) model with the velocity as the input [3]. The Morison formula [2] is applied to calculate the fluid forces on the cylindrical jack-up legs.

2.2 Leg-Seabed Interaction

The leg-seabed interaction is first analyzed with a Finite-Element model. Afterwards, the results are used to develop a mechanical rheological model.

Three-dimensional finite element models using the Coupled Eulerian-Lagrangian (CEL) method [5] are used to investigate the interaction between legs and seabed. The soil is modelled in an Eulerian domain. 3D Eulerian elements with reduced integration (element type: EC3D8R) are used to discretize the soil (see Figure 2a). By shallow penetration ($z < 3.5$ m) the vertical reaction force $\mathbf{q}_{\text{seabed,z}}$ depends only on the penetration depth. The penetration angle has rare influence on the leg-seabed reaction. By contrast, the penetration angle of the leg does have great influence on the horizontal reaction force $\mathbf{q}_{\text{seabed,y}}$, because the horizontal reaction force depends on the contact area of the leg with soil, the depth of the leg and the mobilization of the passive earth pressure. For the same horizontal movement the smaller penetration angle leads to larger contact area, larger penetration depth.

The FE-model is computationally too expensive to be used in stochastic simulations. Therefore, we propose a simple mechanical rheological model for the seabed reaction force, which is based on the FE- results. We use an anelastic model, because the seabed will usually not yield recovery after the stress from the penetrating leg is removed. The plactic material law is represented by nonlinear Coulomb elements in the vertical and horizontal directions, respectively. We denote the penetration depth in vertical direction with $\mathbf{p}_{\text{seabed,z}}$ and the displacement in horizontal direction in relation to the impact point with $\mathbf{p}_{\text{seabed,y}}$.

The nonlinear friction coefficient in z-direction depends on the penetration depth $\mathbf{p}_{\text{seabed,z}}$ only. The reaction force is regarded as a penetration resistance and vanishes as soon as the leg stops or starts moving upwards. The horizontal reaction force can be computed similarly, but the nonlinear friction coefficient depends on the horizontal displacement $\mathbf{p}_{\text{seabed,y}}$ as well as on the penetration depth of the leg $\mathbf{p}_{\text{seabed,z}}$. The horizontal force vanishes for a zero horizontal velocity. The nonlinear friction coefficients are determined from the results of the FE-computations (Figure 2b and 2c) and are implemented as lookup tables with linear interpolation.

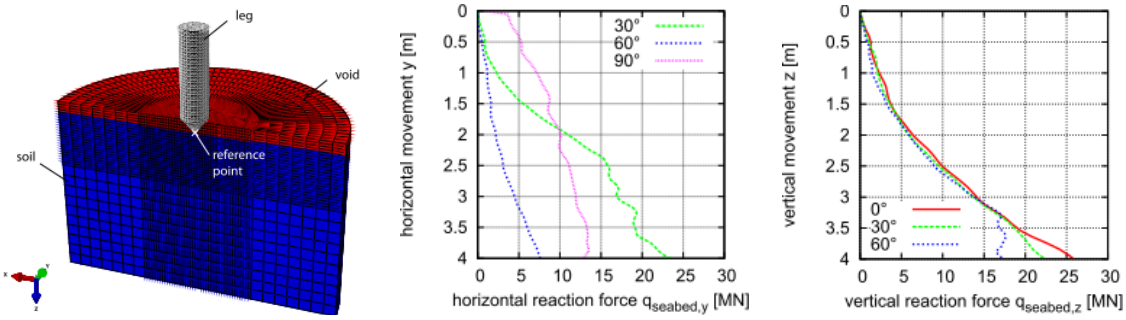

(a) Mesh. (b) Horizontal reaction force. (c) Vertical reaction force.

Fig. 2: FE-Computations with the CEL Model.

3 Results

The JONSWAP spectrum is taken as the spectral density of the stochastic wave-elevation. Three different scenarios with significant wave heights $H_{sig} = 2m$, $H_{sig} = 3m$ and $H_{sig} = 4m$ are analyzed. The peak period amounts for $T_p = 10s$ for all three scenarios. The water depth is $H = 45m$. The distance from the legs to the sea ground is initially $L_l(t_0) = 3m$. The legs are continuously lowered with a speed of $0.5\frac{m}{s}$. We compute 3000×10min random realizations of irregular waves for each scenario and integrate system (1) N = 3000 times for each scenario. As soon as an impact occurs and the maximum impact force in z-direction is reached, the integration is stopped and a new run is started. For each run the maximum force from the seabed on the leg is computed for the case of a contact.

Figure 3 illustrates the empirical cumulative distribution function of the maximum seabed force for the three different scenarios. As one would intuitively expect, higher significant wave heights lead to higher impact forces. The jacking system is designed to carry the weight of the jack-up vessel, which is of the order $\mathcal{O}(10^8 N)$. The impact forces seem to be relatively small being of the order $\mathcal{O}(10^5 N)$. However, the weight is a static load, which is distributed over all legs. The impact force is a dynamic load usually acting on one leg only. Moreover, the jacking system is supposed to bear axial loads. The impact force will in general not act co-axially with the leg, causing bending moments. A detailed structural analysis of the jacking system, subject to the impact force will be topic of further studies.

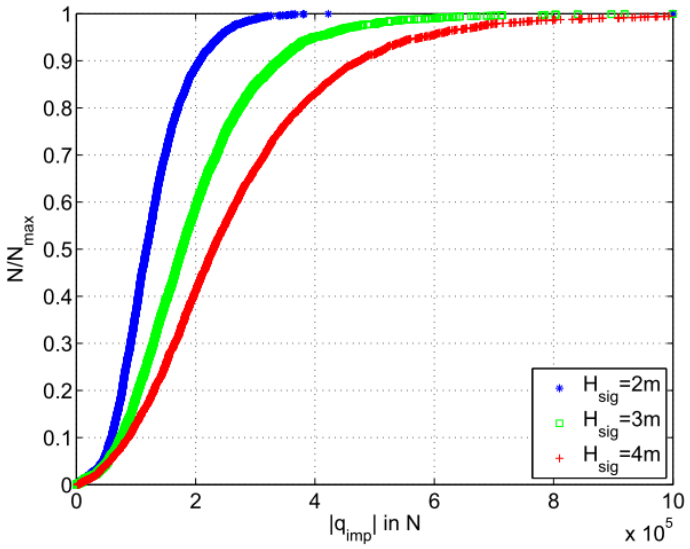

Fig. 3: Empirical cumulative distributions for the amplitude of the impact forces.

Acknowledgment

We gratefully acknowledge the support provided by the Free and Hanseatic City of Hamburg.

References

[1] Cummins, W.: "The impulse response function and ship motions". *Schiffstechnik*, **9**(1661), pp. 101-109, 1962.

[2] Manners, W.; Rainey, R.C.T.: "Hydrodynamic forces on fixed submerged cylinders". *Proc. R. Soc. Lond. A*, **436**, pp. 13–32, 1992.

[3] Perez, T.; Fossen, T.I.: "A matlab toolbox for parametric identification of radiation-force models of ships and offshore structures". *Modeling, Identification and Control*, **30**(1), pp. 1–15, 2009.

[4] Qiu, G.; Henke, S.; Grabe, J.: "Application of a Coupled Eulerian-Lagrangian approach on geomechanical problems involving large deformations". *Computers and Geotechnics*, **38**(1), pp. 30–39, 2011.

Numerical Simulation of the Berthing Manoeuvre of Service Vessels to Offshore Wind Turbine Plants

Marcel König, Eyke Höft, Alexander Düster
Hamburg University of Technology, Institute for Ship Structural Design and Analysis, Numerical Structural Analysis with Application in Ship Technology, Schwarzenbergstraße 95c, D-21073 Hamburg, marcel.koenig@tuhh.de

Once an offshore wind turbine plant requires maintenance or repair, a service team needs to be transferred from a service vessel to the plant. In order to guarantee a safe crew transfer, the relative movement between the ship and the offshore structure must not exceed a critical limit. To this end, the ship is equipped with a fender at its bow, which is pressed against the tower and creates a friction force counteracting the ship's vertical movement in the swell. Our research aims at simulating the berthing manoeuvre to analyze under which conditions a safe transfer of the servicing staff can still be ensured. We present a comprehensive framework for the solution of the governing fluid-structure interaction problem and apply it to a numerical example.

1 Introduction

Due to the high availability needs in the energy industry, offshore wind turbine plants require regular maintenance and occasional repair. In this regard, it is imperative to limit the vertical movement of the service vessel in the swell to allow the servicing crew to transfer safely from the ship to the plant. To this end, a fender is mounted at the ship's bow, which creates a friction force on being pressed against the offshore structure. The landing manoeuvre is governed by the interaction of the swell with the ship's hull and the contact between the fender and the tower. In order to solve this coupled problem, we advocate a partitioned approach, where existing specialized fluid and structural solvers might be reused and coupled via an implicit procedure.

In previous works, we employed the boundary element method (BEM) to discretize the fluid domain and a high order finite element method (FEM) to solve the structural problem [1]. An MPI-based interface was developed to manage the data transfer between the solvers and implement the implicit coupling procedure. Subsequently, the interface was not only applied to fluid-structure interaction [2], but also to thermo-mechanical [3] and mechanical-mechanical [4] problems. We investigated various predictor and relaxation techniques to stabilize the solution algorithm and accelerate its convergence.

In the present work, the fluid domain is discretized by finite volumes, while finite elements are used for the structural domain. The relevant field quantities are exchanged via the coupling interface, which also implements the implicit coupling procedure.

2 Partitioned Approach

A partitioned approach is used to solve the coupled equations of motion. In contrast to a monolithic technique, where an aggregated system of fluid and structural equations needs to be solved, a partitioned scheme is based on the idea of decomposing the domain under consideration into partitions. Interaction is achieved by exchanging the coupled state variables at the interface between the different partitions. In a partitioned scheme, existing dedicated solvers can be reused, which makes the partitioned approach not only very flexible but also easy to implement from a programming point of view. However, appropriate measures must be taken to circumvent stability problems. In this treatise, we use an interface quasi-Newton technique, as outlined in [5].

2.1 Fluid Problem

The fluid is assumed to be Newtonian and incompressible and can thus be described by the incompressible Navier-Stokes equations, which comprise the mass conservation equation and the balance of linear momentum. Due to the difficult nature of the Navier-Stokes equations, instantaneous quantities are decomposed into time-averaged and fluctuating quantities, which results in the Reynolds-averaged Navier-Stokes (RANS) equations, where an appropriate turbulence model is required to model the resulting nonlinear Reynolds stress term and close the RANS equations.

The fluid domain is discretized by a structured or unstructured finite volume mesh. In order to track and locate the free surface, we employ the volume-of-fluid (VOF) approach, which is readily available in commercial and non-commercial software packages. In the present work, we use a modified version of the interDyMFoam solver

from the OpenFOAM toolbox [6], which handles multiphase flows and moving meshes. The time integration is performed using the backward Euler method.

2.2 Structural Problem

The part of the mechanical structure in contact with the fluid is modelled as an isotropic elastic body, which undergoes large displacements and large rotations but only small strains. Since only small strains are considered, a constitutive relation between the second Piola-Kirchhoff stress tensor and the Green-Lagrange strain tensor is established using the Saint Venant-Kirchhoff model, which extends the linear elastic material law to the geometrically nonlinear regime.

The structural domain is discretized by the finite elements using the software ANSYS [7]. The Newmark scheme is employed to integrate the equations of motion with respect to time. Similar to the fluid solver, the structural solver is modified to interface with the coupling software using the ANSYS Parametric Design Language (APDL).

2.3 Coupling Procedure

The fluid and the solid solver are coupled via an MPI-based interface, which implements the coupling algorithm. At the beginning of each time step, a polynomial or least squares predictor step is performed to provide a good initial guess for the fluid loads. In an implicit loop, which is required to stabilize the simulation, the fluid solver first determines the loads on the hull of the vessel before passing the results over to the solid solver, which solves for the rigid body displacement of the vessel and the deformation of the fender. The displacement of the vessel's hull is then passed back to the fluid solver. A relaxation step inside the implicit loop also enhances the stability of the solution algorithm. Besides a static and a dynamic relaxation scheme, we also implemented the quasi-Newton procedure [5], which has been found to perform particularly well in earlier works.

3 Numerical Example

A numerical example adopted from [8] is studied to illustrate the numerical procedure described in the previous section.

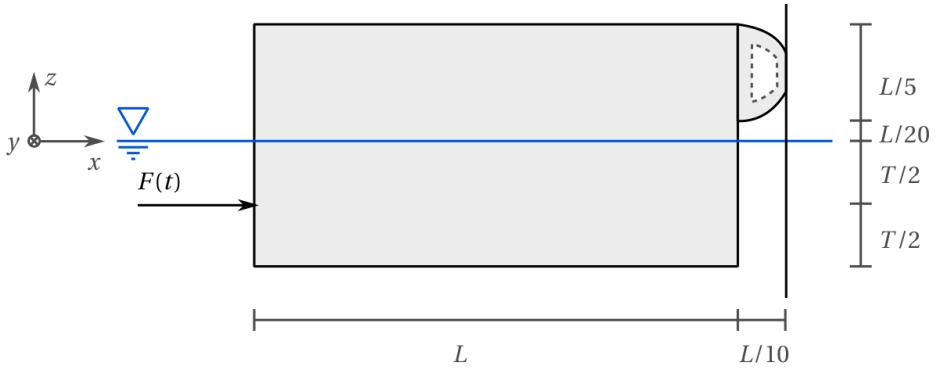

Figure 1: Numerical model of the service vessel.

As depicted in Figure 1, the ship's hull is modelled as a rectangular cuboid of length $L = 1$ m, height $H = 0.5$ m, and width $W = 1$ m. The linear elastic material has a density of $\rho = 500\ \mathrm{kg/m^3}$ and a Young's modulus of $E = 2.1 \cdot 10^{11}\ \mathrm{N/m^2}$. Hence, the initial draft results in $T = 0.5$ m. The ship is driven by a linearly increasing thrust of $F_1(t) = 35\ \mathrm{N/s} \cdot t$ during the first two seconds of the simulation, which is then held constant at $F_2(t) \equiv F_2 = 70$ N. At its bow, the vessel is equipped with a hyperelastic fender made of incompressible Neo-Hookean material, whose strain energy function is given by $W = C_{10}(I_1 - 3)$, where $C_{10} = 388403\ \mathrm{N/m^2}$ is a material parameter and I_1 is the first invariant of the Cauchy-Green strain tensor. The friction between the fender and the tower is assumed to be of Coulomb type, where the vertical friction force F_f is proportional to the horizontal normal force F_n. As long as no relative movement occurs between the fender and the tower, the maximum admissible force is the static friction force $F_\mathrm{s} = \mu_\mathrm{s} F_\mathrm{n}$. Once the fender begins to slide, the dynamic friction force $F_\mathrm{d} = \mu_\mathrm{d} F_\mathrm{n}$ comes into effect. Irrespective of the fact that μ_s and μ_d might be different and might also change over time, it is assumed that $\mu_\mathrm{s} = \mu_\mathrm{d} = \mu = 0.5$ provides a sufficient approximation to the real contact situation. The pontoon and the attached fender are discretized by 2184 and 480 8-noded hexahedral elements, respectively. In addition, the fender is covered with 464 4-noded contact elements, which face 400 rigid target elements on the

tower side. The pontoon is subjected to linear Airy waves, which are characterized by a phase shift $\varphi = 0$ rad, a wave period of $T_w = 1.70$ s, a wave length of $\lambda = 4.5$ m, and a wave height of $H_w = 0.11$ m. The fluid domain is discretized by a structured finite volume mesh, which is very fine in the vicinity of the pontoon.

As illustrated in Figure 2, the ship stays in a comparatively stable position for $0 \leq t \leq 4$ s before the stern starts oscillating heavily. At $t \approx 9$ s, the fender temporarily loses contact with the tower, so the contact force and accordingly the friction force drop to zero. A jump occurs in the displacements at the bow, which, however, then show only slight variations until the end of the simulation. The variations in the contact force imply that the fender almost loses contact but still produces a friction force large enough to keep the bow in position.

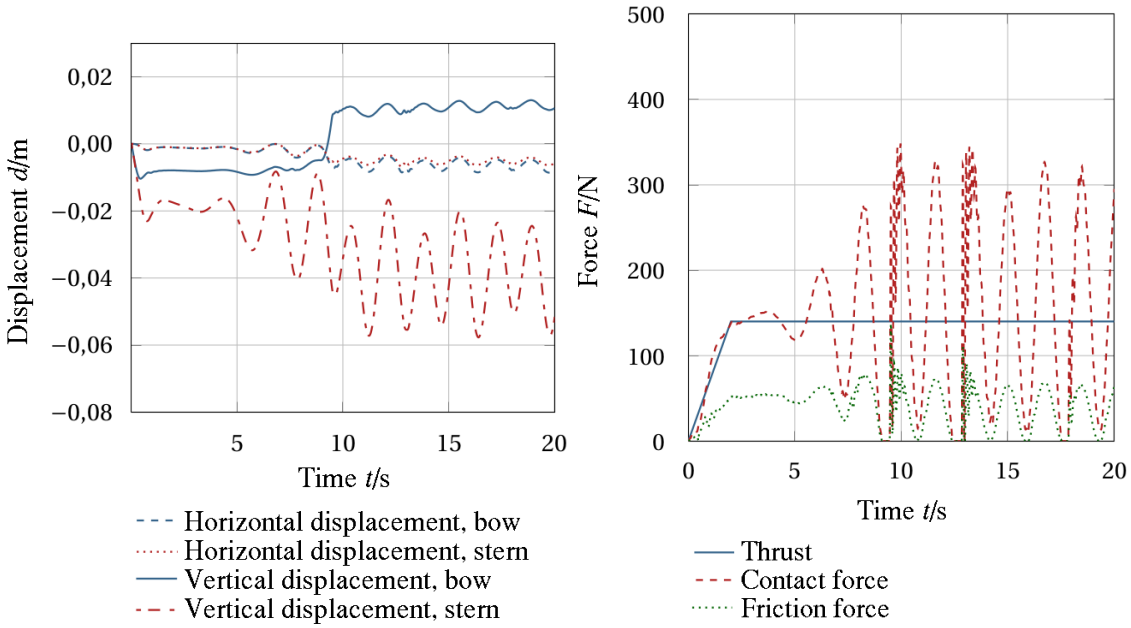

Figure 2: Horizontal and vertical displacements at the bow and the stern (left) and thrust, contact force and friction force at the bow (right).

4 Conclusions and Outlook

In this treatise, a powerful framework for solving fluid-structure interaction problems was presented. Due to the partitioned approach, different solvers might be used for the subproblems and even different discretizations do not pose any difficulties, in principle. In future computations, more elaborate numerical models can be analyzed and will finally allow for a realistic simulation of a real-life berthing manoeuvre.

Acknowledgement

We gratefully acknowledge the support provided by the Free and Hanseatic City of Hamburg.

References

[1] Brändli, S.; Abdel-Maksoud, M.; Düster, A.: A FEM-BEM Approach for Fluid-Structure Interaction. In: *Proc. Appl. Math. Mech.* **11** (2011), 457-458.

[2] Brändli, S;, Düster, A.: A flexible multi-physics coupling interface for partitioned solution approaches. In: *Proc. Appl. Math. Mech.* **12** (2012), 363-364.

[3] Erbts, P.; Düster, A.: Accelerated staggered coupling schemes for problems of thermoelasticity at finite strains. In: *Comput. Math. Appl.* **64** (2012), 2408-2430.

[4] Joulaian, M.; Düster, A.: The hierarchic finite cell method with local enrichment for problems with material interfaces. In: *Comp. Mech.* (2013), 1-22.

[5] Degroote, J.; Bathe, K.-J.; Vierendeels, J.: Performance of a new partitioned procedure versus a monolithic procedure in fluid-structure interaction. In: *Comput. Struct.* **87** (2009), 793-801.

[6] ESI-OpenCFD: OpenFOAM – An open source CFD toolbox, http://www.openfoam.com

[7] ANSYS, Inc.: ANSYS simulation software, http://www.ansys.com.

[8] Höft, E.: Simulation des Anlegemanövers eines Serviceschiffes an einer Offshoreanlage, Diploma thesis (2013).

Numerical Simulations of Ship Motions during Landing Manoeuvres at Offshore Wind Turbine Plants

Daniel Ferreira González
Hamburg University of Technology, Hamburg University of Technology, Institute of Fluid Dynamics and Ship Theory, Schwarzenbergstraße 95c, 21073 Hamburg, Germany, daniel.ferreira@tuhh.de

This paper deals with the development of a numerical method for the simulation of landing manoeuvres of a crew transfer vessel at offshore wind turbine plants. In particular, the last phase of the manoeuvre when the vessel pushes with its fender against the structure is of interest. Therefore, a contact model describing the mechanical interaction between the vessel and the offshore plant is presented. The model which is implemented into the panel code panMARE computes the normal force as well as the friction force due to the boat fender and further determines if either the fender sticks or slips along the contact area. The parameters which characterize the behaviour of the fender are provided by prior structural and numerical fender tests. Finally, simulation results of the described model are shown.

1 Introduction

In the last few years the offshore wind energy industry has rapidly grown and the number of installed wind turbine plants significantly increased. In this course, the effort for repair and maintenance of the systems becomes an important cost factor. One specific aim in this context is the improvement of the accessibility of the plants without endangering the safety for personnel and equipment. The transport of technical employees or equipment to the wind turbine plants is generally done by service vessels. The most critical phase of the transport operation from the safety point of view is when the ship arrives at the offshore platform. Then, the vessel pushes with its bow fender against the structure so that it sticks to the structure and allows the passage if possible. According to this, the accessibility of the plants depends on the prevailing sea condition, but also on the performance of vessel and fender system. As it is not feasible to measure the performance in all sea conditions numerical methods are needed to simulate the landing-manoeuvre and analyse the relative motion. Therefore, in this work a contact model which allows the simulation of the fender-structure interaction is implemented into the fluid solver *panMARE*, which is described in the following section.

2 Short description of the simulation program *panMARE*

The code *panMARE* is a three-dimensional panel method. It allows the simulations of arbitrary potential flows in maritime application. In the program natural sea ways are described as the sum of linear waves defined by the velocity potential Φ_w (see [1]) which respectively differ in their frequency, direction and height. By solving the *Laplace equation*, assuming the fluid to be incompressible and inviscous, the velocity and the pressure distribution on the body surface are obtained which leads to the hydrodynamic forces. Further, a 6-DoF motion model based on *Newton's 2nd law* is implemented which allows the computation of free motions of rigid bodies in six degrees of freedom. Here, the description of rotations refers on the theory of quaternions. For the numerical integration of the accelerations and velocities either an implicit or explicit *Euler method* can be used.

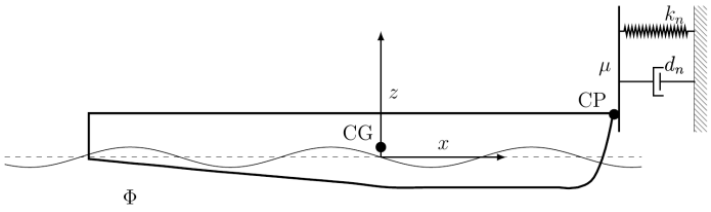

Fig. 1: Sketch of contact model

3 Contact Model

The contact area for the fender is modelled as a vertical plane at the contact point (CP). As in Fig. 1 shown, the area is hinged to a spring-damper-system describing the reaction force in normal direction due to the penetration of the fender and its elastic deformation. Further, forces acting in tangential direction of the contact plane occur because of the surface roughness which is defined by coefficients of friction μ. Whilst the normal force can be easily computed the friction force between fender and the contact plane is relatively more complex to determine,

because it depends on the sum of all acting forces as well as of the current kinetic condition. According to this, a distinction between stick condition and slip condition has to be made. In the following section the computation of the friction force is described in more detail.

3.1 Friction Force

As mentioned before the friction force F_f depends on the condition, whether the fender is currently slipping or it sticks at the structure. During the slip (kinetic) condition the friction force F_{kf} always acts in the opposite direction to the current motion $\dot{x}$ of the fender. Furthermore, the friction can't exceed the absolute force which is needed to stop this tangential motion or to let the fender stuck to the contact area. If a stick condition is achieved a higher friction force F_{sf} can be provided between the surfaces. For this distinction *Coulomb's law of friction* gives the following formulations

$$\left|F_{sf}\right| \leq \mu_s \, |F_n| \tag{1}$$

$$\left|F_{kf}\right| = \mu_k \, |F_n| \tag{2}$$

which describe the respective dependency of the static friction force F_{sf} and the kinetic friction force F_{kf} as a function of the normal force F_n. Here, μ_s and μ_k denote the coefficient of static and kinetic friction, respectively. As in general $\mu_s \neq \mu_k$, this formulation causes a discontinuity for the case of a vanishing velocity v (see Fig. 2). In [2] an extended formulation presented by *Stribeck* [3] is used. Here, the actual transition from static to kinetic friction coefficient is assumed to be of exponential kind. The general representation of *Stribeck's Curve* which is plotted in Fig. 2 is

$$\left|F_f\right| \leq \left(\mu_k + \, (\mu_s - \mu_k) \exp\left(-\left(\frac{v}{v_{ref}}\right)^{\delta}\right) + k_v \, v\right) |F_n| \tag{3}$$

Here, δ is a coefficient to be taken in the range $[0.5, 2.0]$, v_{ref} denotes a reference velocity defining the minimum of the friction coefficient and k_v is a viscous constant which considers the increase of the coefficient due to higher velocities.

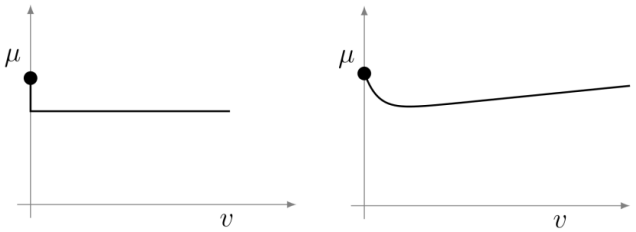

Fig. 2: Friction coefficient plotted against velocity for *Coulomb's law* (left) and for *Stribeck's Curve* (right)

Using Eq. (3), during the stick condition only the maximum available friction force which can be provided by the interaction between the respective surfaces of fender and structure can be calculated. Whereas, the actually required friction force which is necessary to stick the fender or keep it stuck can be much lower than the calculated maximum. To compute this friction force which is actually required not only the current state values are necessary but also the sum of all other acting forces $\sum \boldsymbol{F}_0$. Hence, an additional unknown force vector $\boldsymbol{F}_{f,\mathrm{req}}$ get into the Eq. of motion:

$$\boldsymbol{M}\,\ddot{\boldsymbol{x}} - \boldsymbol{F}_{f,\mathrm{req}} = \sum \boldsymbol{F}_0 \tag{4}$$

where $\ddot{\boldsymbol{x}}$ is the acceleration vector and $\boldsymbol{M}$ the mass matrix. To solve the equations nevertheless a boundary condition defining the condition that the fender is forced to stick in the next time step is added. For this, the velocity $\dot{x}_{CP}$, which defines the motion of the fender in tangential direction to the surface of the contact plane, has to be compensated by the acceleration $\ddot{x}_{CP}$ of the next time step. This leads to following equation:

$$0 = -\dot{x}_{CP}^{(i)} + \ddot{x}_{CP}^{(i+1)} \, \Delta t \tag{5}$$

Here, the index i denotes the time step and Δt defines the time step size. The required force $F_{f,\mathrm{req}}$ for stick condition is then obtained solving the coupled Eqs. (4)-(5). If this force does not exceed the provided force F_f from Eq. (3) the fender sticks to the structure. Otherwise, it slides along the surface.

4 Simulation of Landing-Manoeuvre

The ship used for the simulation of landing-manoeuvres is a mono-hull for high speed crew transfer to offshore installations. The body mesh which is based on a lines plan from [4] and the main dimensions of the vessel are shown in Fig. 3. On the other side, for the offshore plant an arbitrary jacket type foundation is chosen. As the diameter of the jacket foundation elements is small compared to the incoming wave length, the structure can be treated as hydrodynamically transparent. The parameters defining the properties of the fender are chosen according to the results from finite element simulations given in [5].

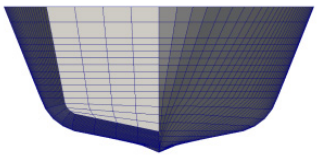

Main dimensions		
Length	28.0 m	
Breadth	5.2 m	
Draught	1.7 m	
Displacement	135	t

Fig. 3: Front/rear view of mesh and main dimensions of a crew transfer vessel.

Here, the motion of the vessel and of its fender is simulated in linear waves ($H_w = 0.5$ m, $T = 5$ s) whilst it pushes against the structure. The direction of propagation of the waves is $\mu_w = 30°$ (see Fig. 4). Several simulations are done varying the propeller thrust force of the vessel. In the right graph in Fig. 5 the vertical motion of the fender is plotted against the time. According the plot, it can be easily distinguished whether and when the fender slips or sticks. It further shows how higher thrust forces support the fender to stick at the structure.

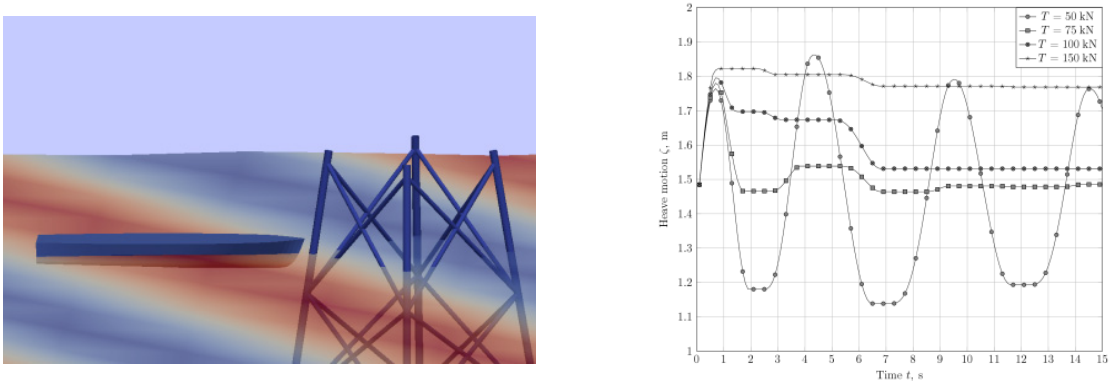

Fig. 4: Simulation of the fender motion during landing manoeuvre at a jacket structure.

5 Summary

A contact model for the simulation of landing-manoeuvres at offshore wind turbine plants has been presented. The results from numerical simulations show it is capable to simulate plausible motions considering the friction between the fender and the structure. However, much more simulations are necessary to evaluate the quality of the described model. Furthermore, the numerical results have to be validated by model tests.

Acknowledgment

We gratefully acknowledge the support provided by the Free and Hanseatic City of Hamburg.

References

[1] Sturm, S.: Berechnung der hydrodynamischen Lasten auf die Fundamente einer Jacket-Struktur mit Hilfe eines Rechenverfahrens für Potentialströmung. Diploma Thesis. Hamburg University of Technology, 2012.

[2] Lemmerhirt, M.: Influence of Friction Forces on Ship Motions during Boat Landing Operations at Offshore Wind Turbines. Diploma Thesis. Hamburg University of Technology, 2013.
[3] Stribeck, R.: Die Wesentlichen Eigenschaften der Gleit- und Rollenlager. Zeitung des VDI, 46, 1902.
[4] Journée, J.M.J.: *Website of Johan Journée*, www.shipmotions.nl.
[5] Kröger, T.: *Numerische Untersuchung eines Fenders von Offshore-Serviceshiffen*. Bachelor thesis. Hamburg University of Technology, 2013.

Ein szenariobezogenes Auswahlverfahren für Augmented-Reality-Komponenten

Philipp Sebastian Halata, Axel Friedewald, Hermann Lödding
Technische Universität Hamburg-Harburg, Institut für Produktionsmanagement und –technik, Denickestraße 17, D-21073 Hamburg, philipp.halata@tuhh.de

Augmented Reality (AR) kann die Durchführung von Tätigkeiten durch Einblenden von Informationen in den Sichtbereich unterstützen. Unterschiedliche Geräte bieten dabei je nach Anwendungszweck unterschiedliche Vor- und Nachteile. Nicht immer ist die Entscheidung für ein Gerät einfach, da sich die Anforderungen des Anwendungszwecks nicht direkt in Gerätespezifikationen übertragen lassen. Diese Arbeit stellt eine systematische, modulare Auswahllogik bereit, die es Entscheidungsträgern vereinfachen soll, geeignete AR-Geräte je nach Anwendungszweck auszuwählen. Expertenwissen ist dabei in einer Matching-Matrix festgehalten, die zwischen Gerätespezifikationen und Anforderungen vermittelt.

1 Augmented Reality

Augmented Reality (AR) [3] kann Benutzern in vielen Bereichen die Durchführung von Tätigkeiten vereinfachen [1]. Dazu werden Informationen – bspw. in Form vom Geometriemodellen oder Text – direkt in die Umgebung eingeblendet. Dies erleichtert z. B. Wartungsarbeiten im Automobilbau [2] oder Alltagsaufgaben wie das Auswechseln einer Druckerpatrone. Das BMWi-Verbundprojekt PROSPER, in dessen Rahmen diese Arbeit entstanden ist, hat zum Ziel, Mitarbeitern der schiffbaulichen Unikatfertigung Montageinformationen per AR zur Verfügung zu stellen. In mehreren Szenarien sollen den Werftmitarbeitern Rohrisometrien oder Zusatzinformationen zu Standardbauteilen, wie etwa Rohrdurchmesser oder Fließrichtung, eingeblendet werden.

Geräte, die für AR zum Einsatz kommen, sind vielfältig: Auf nahezu jedem Smartphone oder Tablet-Computer lässt sich ein um Zusatzinformationen angereichertes Kamerabild anzeigen. Gleiches gilt für Notebooks und Workstations mit Kamera. AR-Brillen ermöglichen es, die Informationen direkt in das Sichtfeld des Benutzers einzublenden. Darüber hinaus können Projektoren die Informationen direkt in der Umgebung anzeigen. Da je nach Anwendungszweck sehr unterschiedliche Anforderungen zu erfüllen sind, gibt es kein AR-Gerät, das überall gleichermaßen geeignet ist.

Aufgrund der hohen Anzahl an Herstellern und Modellen ist es zeitaufwändig, die Spezifikationen jedes einzelnen Geräts mit den Anforderungen abzugleichen und nahezu unmöglich, das objektiv bestgeeignete Gerät auszuwählen. Auch herkömmliche Auswahlverfahren wie etwa die Nutzwertanalyse [5] genügen nicht, da der Zusammenhang zwischen einer gestellten Anforderung (bspw. *Anzeigen komplexer Geometrie und einigen Zusatzinformationen in einer Werftumgebung*) und Gerätespezifikationen (bspw. *1,7 GHz, vier Rechenkerne, Bluetooth-Schnittstelle und kapazitives Touchdisplay*) nicht offensichtlich ist. Zudem lassen sich Anforderungen oft auf unterschiedlichen Wegen erfüllen. Visuelle Objekterkennung kann bspw. einerseits offline auf dem Endgerät oder aber online auf einem Server ausgeführt werden. Das Gerät benötigt also eine Kamera und eine hohe Rechenleistung bzw. eine Datenverbindung.

Diese Problematik macht eine Auswahllogik erforderlich, die die Anforderungen des Anwendungszwecks mit den Gerätespezifikationen verknüpft und eine Antwort auf die Frage liefert: *Welches Gerät erfüllt die Anforderungen des Anwendungszwecks am besten?*

2 Auswahllogik

Die entworfene Auswahllogik beruht in ihren Grundzügen auf der Nutzwertanalyse, um deren Einfachheit und Objektivität beizubehalten. Sie wurde um ein Matching-Verfahren zwischen den Anforderungen des Szenarios und den Gerätespezifikationen erweitert, das die Erfüllungsgrade der einzelnen Anforderungen ermittelt. Die Logik ist schematisch in Abbildung 1 zu sehen.

In der Auswahllogik sind Daten in drei Hauptkomponenten hinterlegt: in Listen mit Geräteeigenschaften, in szenariospezifischen Anforderungen und in der Matching-Matrix. Diese beschreibt, auf welche Weise sich Geräteeigenschaften auf die Erfüllung der Anforderungen auswirken.

Geräteeigenschaften sind in drei Kategorien unterteilt:

Anzeige (z. B. Grafikleistung, Darstellungsart und Anzeigegröße)

Schnittstellen (z. B. Tastaturart, 2D-Kamera-Auflösung und WLAN)

physische Eigenschaften (z. B. Gewicht, Robustheit, Einhand-/Zweihand-Interaktion)

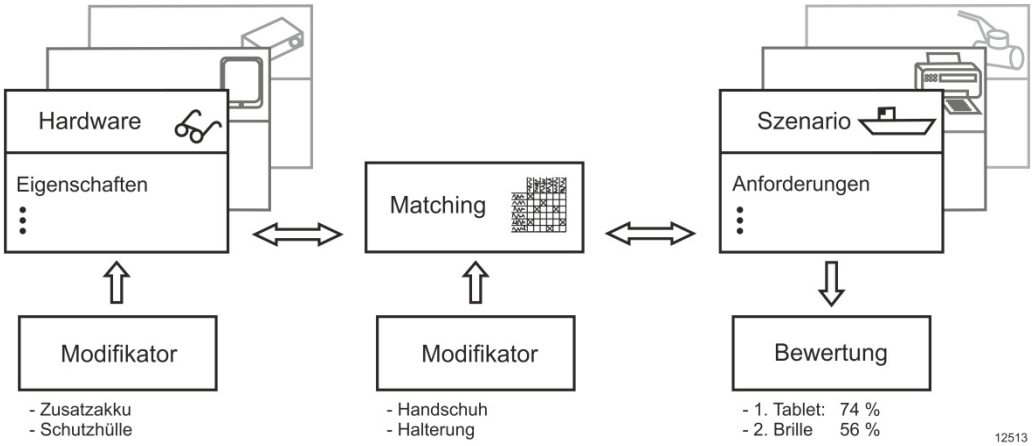

Abb. 1: Schematische Darstellung der Auswahllogik

Jede Eigenschaft enthält mindestens einen Wert (für die Darstellungsart bspw. *Display*, *Projektion* oder *see-through* für die Tastaturart *kapazitiv*, *resistiv* oder *Hardware*), den ein Gerät entweder erfüllt oder nicht. Diesen booleschen Wert verarbeitet das Matching-Verfahren.

Geräte einer Klasse wie Tablet-Computer oder Notebook haben meist gemeinsame Eigenschaften, können sich voneinander aber in anderen Eigenschaften unterscheiden. Es ist daher vorgesehen, zunächst die Geräteklassen zu vergleichen, um eine Grundauswahl zu treffen. Anschließend kann innerhalb der Klasse ein Gerät ausgewählt werden, indem die Eigenschaften gerätespezifisch detailliert werden.

Die szenariospezifischen Anforderungen sind in Kategorien unterteilt, die jeweils Oberziele enthalten:

Anzeige (Geometriekomplexität, -größe, Anzahl an Zusatzinformationen etc.)

Funktionalität (Zweck der Benutzereingabe, Objekterkennung, mobile Kommunikation etc.)

Einsatzbedingungen (Umfeld, Mobilitätsbereich, freie Hände bei der unterstützten Tätigkeit etc.)

Oberziele sind weiter in Teilziele (für den Zweck der Benutzereingabe bspw. *Schreiben*, *Kurzbefehle* und *Geometrieinteraktion*, für das Umfeld *Büro*, *Produktion* und *Outdoor*) aufgeteilt, die der Benutzer der Auswahllogik je nach Szenario in eine der Anforderungsklassen *muss*, *soll* oder *kann* einordnet.

Die Matching-Tabelle verbindet schließlich die Geräteeigenschaften und die Anforderungen. Dabei müssen folgende Fälle abgedeckt sein:

Eigenschaft P ermöglicht Anforderung A:
WLAN ermöglicht eine *hohe Datenmenge an mobiler Kommunikation.*

Eigenschaft P_1 oder P_2 ermöglichen Anforderung A:
Maus oder *kapazitives Touch-Display* ermöglichen *Geometrie-Interaktion.*

Eigenschaft P_1 und Q_1 ermöglichen Anforderung A:
Geringes Gewicht und *lange Akkulaufzeit* ermöglichen eine *lange Mobilitätsdauer.*

Mit der konjunktiven Normalform (KNF) [4] lässt sich jeder dieser Fälle sowie jede Kombination daraus darstellen. Die Erfüllung A_{Erf} einer Anforderung A ist damit definiert als

$$A_{Erf} = (P_1 \vee \ldots \vee P_n) \wedge \ldots \wedge (Q_1 \vee \ldots \vee Q_n) \quad (1)$$

Die Indizes der KNF sind in der Matching-Matrix festgelegt. Die Zeilen der Matrix entsprechen den Geräteeigenschaften, die Spalten den Anforderungen. Ein Experte muss die Matrix einmalig befüllen.

Damit ein Gerät für ein Szenario in Frage kommt, müssen alle Muss-Anforderungen erfüllt sein. Welches Gerät sich am besten für das Szenario eignet, entscheidet sich über die Soll- und Kann-Anforderungen. Diese fließen mit zusammen jeweils 75 bzw. 25 Prozent in die Bewertung eines Gerätes ein, anhand derer die Reihenfolge der Eignung der verschiedenen Geräte gebildet wird.

3 Modifikatoren

Oftmals erscheint ein Gerät für ein Szenario zunächst ungeeignet, eignet sich jedoch in Verbindung mit Hilfsmitteln. So kann bspw. ein Gerät, für dessen Bedienung zwei Hände erforderlich sind, bei Verwendung einer Halterung mit einer Hand bedient werden. Geräte lassen sich in Kombination mit einem wasserdichten Gehäuse ggf. auch im Außenbereich einsetzen, ein Zusatzakku verändert Betriebsdauer und Gewicht. Ebenso kann die Eig-

nung eines Gerätes in Verbindung mit Hilfsmitteln auch sinken. Ein Beispiel dafür sind Schutzhandschuhe, mit denen sich ein kapazitives Touch-Display nicht mehr bedienen lässt.

Diese Hilfsmittel nehmen als *Modifikatoren* Einfluss auf das Ergebnis. Modifikatoren können an zwei Punkten angreifen: Geräte-Modifikatoren (wie ein Zusatzakku oder eine Schutzhülle) beeinflussen direkt die Gerätespezifikationen; Matching-Modifikatoren (wie eine Halterung oder Handschuhe) verändern das Zusammenwirken innerhalb des Szenarios, also die Matching-Matrix.

4 Validierung

Zur Validierung des Konzeptes sollen drei beispielhafte Einsatzzwecke dienen: Verbau von Rohrisometrien im Schiffbau, das Einblenden von Zusatzinformationen zu Bauteilen in einem Zwischenlager und der Patronenwechsel bei einem Drucker. In Tabelle 1 sind die Anforderungsklassen für die drei Szenarien zu sehen. Der Übersicht halber sind einige Anforderungen ausgeblendet.

Tab. 1: Anforderungen der drei Beispielszenarien

M = Muss-Anforderung S = Soll-Anforderung K = Kann-Anforderung	Geometrie-Komplexität			Geometrie-Größe			Anzahl Zusatz-informationen			Dokument-größe			Benutzer-eingabe				Objekt-erkennung		Umfeld			Mobilitäts-bereich			Mobilitäts-dauer			Freihändigkeit bei Benutzung	
	gering	mittel	hoch	klein	mittel	groß	wenige	mittel	viele	klein	mittel	groß	Bestätigen	Kurzbefehle	Schreiben	3D-Interaktion	2D	3D	Büro	Produktion	Outdoor	klein	mittel	groß	kurz	mittel	lang	1 Hand	2 Hände
Rohrisometrien	M	M	M	M	M	M	M	M	K	M	M	S	M	M	S	K	M	K	S	M	K	M	M	S	M	M	S	S	K
Zusatzinformationen	K	K	K	K	K	K	M	S	K	S	S	K	K	K	K	K	M	K	S	S	K	K	K	K	K	K	K	K	K
Patronenwechsel	M	S	K	M	S	K	M	K	K	K	K	K	M	M	K	K	M	K	M	K	K	M	M	M	M	K	K	M	K

Die Auswertung der Ergebnisse für die Geräteklassen ist in Tabelle 2 dargestellt. Um Rohrisometrien im Schiffbau einzublenden, zieht die Auswahlsystematik Tablet-Computer mit speziellen Touch-Display-Handschuhen AR-Brillen vor. Um stationär Zusatzinformationen zu Bauteilen anzuzeigen, eignet sich eine einfache Workstation mit Kamera und Monitor, für eine Assistenz beim Patronenwechsel in einer Büroumgebung ein leichtes Smartphone. Dieses Ergebnis kann weiter detailliert werden, um jeweils ein Modell auszuwählen, indem das gleiche Vorgehen auf die einzelnen Geräte angewendet wird.

Durch den modularen Aufbau lassen sich neben weiteren Szenarien auch neu erscheinende Geräte oder sogar Geräteklassen und Modifikatoren in die Auswahllogik einpflegen.

Tab. 2: Bewertung der Hardware für die drei Beispielszenarien

Rohrisometrien	
1. Tablet	66%
2. Smartphone	60%
3. Brille	45%

Zusatzinformationen	
1. Workstation	92%
2. Tablet	78%
3. Smartphone	65%

Patronenwechsel	
1. Smartphone	91%
2. Brille	88%
3. Tablet	68%

Danksagung

Das Forschungsprojekt PROSPER (Förderkennzeichen 03SX337A) wurde gefördert vom Bundesministerium für Forschung und Technologie (BMWi) aufgrund eines Beschlusses des Deutschen Bundestags.

Literaturverzeichnis

[1] Alt, T.: Augmented Reality in der Produktion, Herbert Utz Verlag München, 2002.

[2] Bade, C.: Untersuchungen zum Einsatz der Augmented-Reality-Technologie für Soll/Ist-Vergleiche von Betriebsmitteln in der Fertigungsplanung, LogosVerlag Berlin, 2010.

[3] Milgram, P.: Augmented Reality: A class of displays on the reality virtuality continuum, 1994.

[4] Rautenberg, W.: Einführung in die mathematische Logik, Vieweg + Teubner Wiesbaden, 2008.

[5] Zangemeister, C.: Nutzwertanalyse in der Systemtechnik – Eine Methodik zur multidimensionalen Bewertung und Auswahl von Projektalternativen, Dissertation, Technische Universität Berlin, 1970

.

Fast Numerical Calculation Methods for the Investigation of Real Ship Accidents

Hendrik Dankowski
Hamburg University of Technology, Institute of Ship Design and Ship Safety, Schwarzenbergstraße 95c, 21073 Hamburg, Germany, dankowski@tuhh.de

This short paper describes the task to investigate real ship accidents in an efficient and comprehensive way from an engineering point of view. The applied numerical methods are described briefly together with a short summary of some interesting accident investigations.

1 Introduction

The investigation of real ship accidents is mandatory to identify the root causes, which lead to these tragic events. It is required to establish and apply numerical methods, which are accurate enough, reliable and fast at the same time. The requirements of such methods are similar to methods for the early ship design, for software applied in the salvage business or methods used in emergency response systems.

The task for the engineer and the applied numerical method is always to be as fast as possible without neglecting the most contributing factors. Another challenge of accident investigations is the fact that the required data for the computational models might be incomplete or even missing.

Especially new technologies like the installation of offshore wind turbines require an interdisciplinary approach to gain knowledge about all fields of engineering science involved in this task. The investigation of accidents may have to consider influences from the topography of the seabed, special manoeuvring behaviour, structural engineering and complex flow computations.

2 Numerical Methods

The most severe ship accidents are caused either by capsizing in very rough weather conditions, large scale flooding incidents, the outbreak of fire or a combination of these threats.

The first numerical methods to assess such events has been started to develop right after the beginning of the first modern computer architectures in the seventies, even though the ideas and the underlying theory are much older. It should be stressed that especially at the beginning of the application of numerical methods in engineering, very efficient and powerful methods has been developed. The available computer power was limited and it was the task of the engineer to exactly specify the required scope of the numerical computations.

In the following, two methods are briefly addressed: complex flooding simulations in the time domain and the computation of internal floodwater dynamics. An additional good overview of numerical methods for ship safety problems can be found in [12].

2.1 Numerical Flooding Calculations

One of the most severe threats to modern ships is a rupture to its watertight integrity, which lead to the spread of water through the inner subdivision of the vessel. Today it is tried to minimize the risk of damage and water ingress by the regulations, which require for each vessel to fulfil a probabilistic requirement. However, one major problem is that these requirements are only for newbuildings and that recent accidents like the one of the COSTA CONCORDIA in 2012 show that a combination of human factors and insufficient survivability of a vessel against damage still lead to very severe accidents.

The large scale flooding of ships mainly occur in waterways close to the shore with high traffic. This means that the influence of rough seaway conditions can be in many cases neglected. In addition, flooding incidents in very rough weather conditions are in the later phase mainly triggered by the progressive distribution of the floodwater. The additional water mass leads to a significant damping of the ships motion.

Motivated by this consideration, a quasi-static numerical flooding simulation has been developed by Dankowski [2]. A hydraulic model for the water flow through the openings is applied. The inner subdivision and the possible paths for the ingressed floodwater can be very complex and requires a comprehensive description. This is done by the application of directed graphs. The nodes of the graph are the compartments of the ship connected by the openings, which are modelled by the edges of the graph.

Further aspects included in the numerical model are the breaking and leakage of openings like collapsing doors, compressed air pockets and additional moments caused by the influence of wind or cargo shift. The integration

of the ordinary differential equation, which describes the propagation of water is performed with a predictor corrector scheme to account for the nonlinearity of the problem. At each time step, the new distribution of the floodwater is computed followed by a quasi-static determination of the new equilibrium floating position of the vessel. The explicit and direct computation leads to a fast runtime which allows to study various different scenarios within a short time.

2.2 Shallow Water Computations Inside a Moving Ship

The dynamic motion of the vessel in an accident situation might play an important role, especially in the early transient phase of flooding and in the present of larger waves. In this case, the stability and the motion of the vessel is influenced by the moments induced by the internal floodwater dynamics. The motion of this floodwater can be described by different levels of complexity as described for example in [11]. The most violent motions of the water occurs if the exciting frequency is close to the natural frequency of the tanks. Because this is most often the case when the water is shallow, this can be numerically computed by a solution of the shallow water equations. The occurrence of hydraulic jumps require an efficient and stable numerical solution scheme.

An application of Glimm's random-choice method [5] on this problem has first been described in Dillingham [4] and implemented by Petey [9] to allow the coupling with the nonlinear seakeeping code E4-ROLLS [7]. The external accelerations by the moving ship induces the motion of the trapped floodwater. In addition, boundary conditions like the in- or outflow of water through leaks have to be considered. Alternative methods for an efficient and stable solution of the shallow water equations are for example described in Janßen et al. [6] or Kurganov and Petrova [8].

3 Investigations

3.1 The Might Servant 3 Accident

The semi-submersible vessel MIGHT SERVANT 3 sunk to the seabed during a ballast operation in the morning of December 6, 2006 near the coast of Angola. The first difficulty was to reconstruct a data model from the sparely available information about the vessel. A very useful source was the record from the Maritime Disciplinary Court of the Netherlands, who performed the official investigation of this accident.

What makes this accident especially interesting is the multi-body interaction of the vessel with the loaded platform and the seabed at the time of grounding. The numerical flooding simulation is extended by inserting spring elements to model both interactions. As soon as parts of the vessel submerge below the seabed, a linear reaction force is applied to take into account the restriction by the seabed. The interaction with the cargo are considered by extending the solution for the quasi-static equilibrium from three to six degrees of freedom of the two floating and interacting objects, the vessel and the ship. A few snapshots of the most likely flooding sequence is shown in Fig. 1, while more details on this investigation can be found in [3].

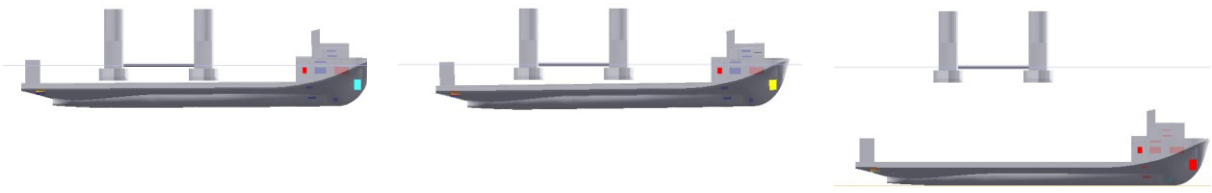

Figure 1: Time steps from the Animation of Submerging

3.2 The Costa Concordia Accident

The ship accident of recent times, which draw the most public interest is probably the flooding and sinkage of the Costa Concordia close to the shore of the Italian island Giglio on January 13, 2012. A thoroughly investigation of the flooding sequence is published by Russell [10].

The fast runtime of the numerical method allows to study multiply different scenarios within a short time. Examples for such scenario studies are shown in Fig. 2 where the most likely flooding sequence is compared to a reference scenario and the case when no second grounding would have occurred. This shows that the ship would have capsized rapidly after around 15 minutes on the open sea.

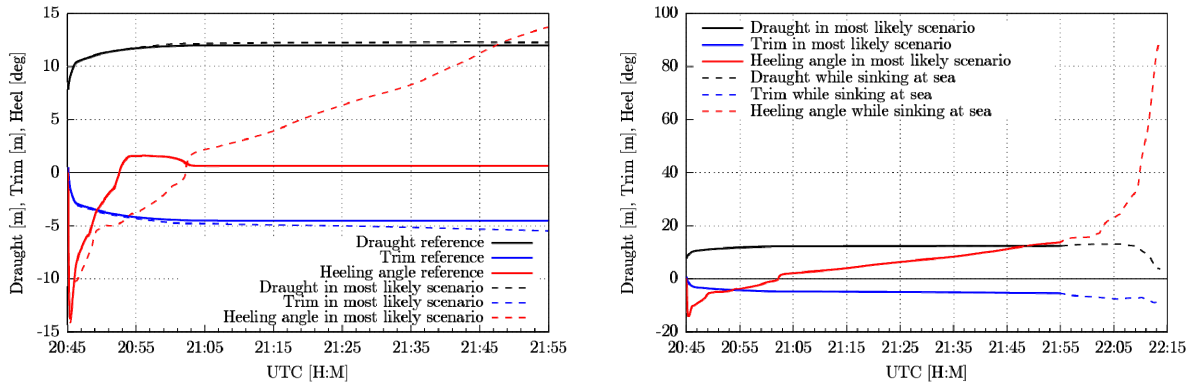

(a) Most Likely Scenario

(b) Sinking at Sea

Figure 2: Development of the ships motion over time during the accident

4 Conclusions

Each accident investigation requires tailor-made numerical software solutions to take into account the various different effects, which played a vital role for the timeline of events leading to the failure of the involved systems. The investigation itself is required to learn from these failure modes and improve the safety of ships. Furthermore, only the investigation of full scale accidents allows to verify the developed numerical methods in an elaborate way. Each accident may reveal new effects, which has to be taken into account and show the most important aspects to focus on. This allows to develop and improve fast numerical methods for the use in the industry in various application fields.

Furthermore, it is essential to address the task of accident investigations with an interdisciplinary approach. The input from all maritime engineering sciences is required to gain a complete and elaborate numerical model to reconstruct the correct accident scenario within an appropriate time.

Acknowledgment

We gratefully acknowledge the support provided by the Free and Hanseatic City of Hamburg.

References

[1] ASME: 32nd International Conference on Ocean, Offshore and Arctic Engineering, Number 32, Nantes, France. ASME, 2013.

[2] Dankowski, H.: A Fast and Explicit Method for the Simulation of Flooding and Sinkage Scenarios on Ships. Ph.D. Thesis, Hamburg University of Technology, Institute of Ship Design and Ship Safety. ISBN 978-3-89220-668-2, 2013.

[3] Dankowski, H.; Dilger, H.: Investigation of the Mighty Servant 3 Accident by a Progressive Flooding Method. In OMA, 2013.

[4] Dillingham, J.: Motion Studies of a Vessel with Water on Deck. Marine Technology. 1981.

[5] Glimm, J.: Solutions in the large for nonlinear hyperbolic systems of equations. Communications on Pure and Applied Mathematics, 18(4):697–715, 1965.

[6] Janßen, C.; Bengel, S.; Dankowski, H.; Rung, T.: A Fast Numerical Method for Internal Flood Water Dynamics to Simulate Water on Deck and Flooding Scenarios of Ships. In OMAE, 2013.

[7] Kröger, H.-P.: Simulation der Rollbewegung von Schiffen im Seegang. Schriftenreihe Schiffbau 473, Universitätsbibliothek der TUHH, Hamburg, 1987.

[8] Kurganov, A.; Petrova, G.: A Second-Order Well-Balanced Positivity Preserving Central-Upwind Scheme for the Saint-Venant System. Communications in Mathematical Sciences, 5(1):133–160. Mathematical Reviews number (MathSciNet): MR2310637; Zentralblatt MATH identifier: 05232062, 2007.

[9] Petey, F.: Berechnung der Flüssigkeitsbewegung in teilgefüllten Tanks und Leckräumen. Schriftenreihe Schiffbau, (447), 1984.

[10] Russell, P.: The Sinking Sequence of M.V. Costa Concordia. Master's thesis, Institute of Ship Design and Ship Safety, Hamburg University of Technology, 2013.

[11] Söding, H.: Leckstabilität im Seegang. Number 429. Institut für Schiffbau, Hamburg, 1982.

[12] Söding, H.: Flow computations for ship safety problems. Ocean Engineering, 29:721–738, 2002.